Original

Knist, S.; Goergen, K.; Buonomo, E.; Christensen, O.B.; Colette, A.; Cardoso, R.M.; Fealy, R.; Fernandez, J.; Garcia-Diez, M.; Jacob, D.; Kartsios, S.; Katragkou, E.; Keuler, K.; Mayer, S.; Meijgaard, E.van; Nikulin, G.; Soares, P.M.M.; Sobolowski, S.; Szepszo, G.; Teichmann, C.; Vautard, R.; Warrach-Sagi, K.; Wulfmeyer, V.; Simmer, C.:

Land-atmosphere coupling in EURO-CORDEX evaluation experiments

Journal of Geophysical Research : Atmospheres (2017) AGU

DOI: 10.1002/2016JD025476

AGU PUBLICATIONS

JGR

Journal of Geophysical Research: Atmospheres

RESEARCH ARTICLE
10.1002/2016JD025476

Key Points:
- Spatial patterns, seasonal cycles, and interannual variability of coupling related soil moisture and surface fluxes are reproduced
- EURO-CORDEX RCMs agree in large-scale weak and strong coupling regimes while there is large variability in the transition zone
- In comparison to FLUXNET and GLEAM data the RCMs show a clear tendency toward overestimating coupling strength

Correspondence to:
S. Knist,
sknist@uni-bonn.de

Citation:
Knist, S., et al. (2017), Land-atmosphere coupling in EURO-CORDEX evaluation experiments, *J. Geophys. Res. Atmos.*, *122*, 79–103, doi:10.1002/2016JD025476.

Received 8 JUN 2016
Accepted 3 DEC 2016
Accepted article online 9 DEC 2016
Published online 7 JAN 2017

Land-atmosphere coupling in EURO-CORDEX evaluation experiments

Sebastian Knist[1,2,3], Klaus Goergen[3,4], Erasmo Buonomo[5], Ole Bøssing Christensen[6], Augustin Colette[7], Rita M. Cardoso[8], Rowan Fealy[9], Jesús Fernández[10], Markel García-Díez[10,11], Daniela Jacob[12], Stergios Kartsios[13], Eleni Katragkou[13], Klaus Keuler[14], Stephanie Mayer[15], Erik van Meijgaard[16], Grigory Nikulin[17], Pedro M. M. Soares[8], Stefan Sobolowski[15], Gabriella Szepszo[18], Claas Teichmann[12], Robert Vautard[19], Kirsten Warrach-Sagi[20], Volker Wulfmeyer[20], and Clemens Simmer[1,4]

[1]Meteorological Institute, University of Bonn, Bonn, Germany, [2]Jülich Supercomputing Centre, Research Centre Jülich, Jülich, Germany, [3]Centre for High-Performance Scientific Computing in Terrestrial Systems, Geoverbund ABC/J, Jülich, Germany, [4]Agrosphere (IBG-3), Research Centre Jülich, Jülich, Germany, [5]Met Office Hadley Centre, Exeter, UK, [6]Danish Meteorological Institute, Copenhagen, Denmark, [7]French National Institute for Industrial Environment and Risks (INERIS), Verneuil-en-Halatte, France, [8]Instituto Dom Luiz, Faculdade de Ciências, Universidade de Lisboa, Lisbon, Portugal, [9]Department of Geography, Maynooth University, Maynooth, Ireland, [10]Meteorology Group, Department of Applied Mathematics and Computer Science, Universidad de Cantabria, Santander, Spain, [11]Institut Català de Ciències del Clima, Barcelona, Spain, [12]Climate Service Center Germany (GERICS), Helmholtz-Zentrum Geesthacht, Hamburg, Germany, [13]Department of Meteorology and Climatology, School of Geology, Aristotle University of Thessaloniki, Thessaloniki, Greece, [14]Chair of Environmental Meteorology, Brandenburg University of Technology (BTU), Cottbus, Germany, [15]Uni Research Climate, Bjerknes Center for Climate Research, Bergen, Norway, [16]Royal Netherlands Meteorological Institute (KNMI), De Bilt, Netherlands, [17]Swedish Meteorological and Hydrological Institute, Norrköping, Sweden, [18]Hungarian Meteorological Service, Budapest, Hungary, [19]Laboratoire des Sciences du Climat et de l'Environnement (LSCE), Institut Pierre Simon Laplace, Gif-sur-Yvette, France, [20]Institute of Physics and Meteorology, University of Hohenheim, Stuttgart, Germany

Abstract Interactions between the land surface and the atmosphere play a fundamental role in the weather and climate system. Here we present a comparison of summertime land-atmosphere coupling strength found in a subset of the ERA-Interim-driven European domain Coordinated Regional Climate Downscaling Experiment (EURO-CORDEX) model ensemble (1989–2008). Most of the regional climate models (RCMs) reproduce the overall soil moisture interannual variability, spatial patterns, and annual cycles of surface exchange fluxes for the different European climate zones suggested by the observational Global Land Evaporation Amsterdam Model (GLEAM) and FLUXNET data sets. However, some RCMs differ substantially from FLUXNET observations for some regions. The coupling strength is quantified by the correlation between the surface sensible and the latent heat flux, and by the correlation between the latent heat flux and 2 m temperature. The first correlation is compared to its estimate from the few available long-term European high-quality FLUXNET observations, and the latter to results from gridded GLEAM data. The RCM simulations agree with both observational datasets in the large-scale pattern characterized by strong coupling in southern Europe and weak coupling in northern Europe. However, in the transition zone from strong to weak coupling covering large parts of central Europe many of the RCMs tend to overestimate the coupling strength in comparison to both FLUXNET and GLEAM. The RCM ensemble spread is caused primarily by the different land surface models applied, and by the model-specific weather conditions resulting from different atmospheric parameterizations.

1. Introduction

Land-atmosphere coupling is an important component of the climate system. Through the exchange of energy, mass, and momentum at the Earth's surface, land-atmosphere coupling affects boundary layer evolution, convection, and cloudiness, which in turn affect precipitation generation and the intensity and duration of heat waves. These exchange processes are controlled both directly and indirectly by atmospheric conditions. In general, land-atmosphere coupling strength can be defined as the degree to which the atmosphere responds to anomalies in the land surface state [*Koster et al*., 2006]. Several metrics have been defined for quantifying this coupling strength depending on the variables involved and the feedback processes addressed, e.g., by *Seneviratne et al*. [2006], *Dirmeyer* [2011], *Findell et al*. [2011], *Miralles et al*. [2012], and *Decker et al*. [2015].

A key state variable of the land-atmosphere system is soil moisture, which controls the flux partitioning between sensible and latent heat to a large extent [*Seneviratne et al*., 2010]. Soil moisture-temperature feedback is strongest in transition zones between wet and dry climates. In a wet, energy-limited regime, soil moisture content is always sufficiently high; thus, evapotranspiration is primarily limited by net radiation and the state of the planetary boundary layer. In a dry, moisture-limited regime, the atmospheric moisture deficit cannot be entirely compensated by moisture supply from the land surface via evapotranspiration; i.e., the latent heat flux is constrained by the soil moisture content. The understanding of land-atmosphere coupling processes and its impacts across spatial and temporal scales has continuously improved through observations and modeling. Based on multimodel experiments of the Global Land-Atmosphere Coupling Experiment (GLACE), *Koster et al*. [2006] have identified so-called "hot spot" regions of strong coupling on the global scale for boreal summer. On the local scale, land-atmosphere coupling has been investigated in the context of diurnal boundary layer evolution [*Mengelkamp et al*., 2006; *Santanello et al*., 2009, 2013; *Milovac et al*., 2016] and cloud formation [*Betts et al*., 2015], all of them including observations. Effects of soil moisture-temperature coupling have been investigated on the climatological and daily time scale with positive feedback on the development of heat waves [*Fischer et al*., 2007; *Miralles et al*., 2012; *Hirschi et al*., 2014]. Soil moisture-precipitation coupling shows positive and negative feedback mechanisms on global and local scales [*Hohenegger et al*., 2009; *Taylor et al*., 2012; *Froidevaux et al*., 2014; *Rahman et al*., 2015]. *Guillod et al*. [2013] reveal that this feedback not only depends on the amount of soil moisture but also on its temporal and spatial distribution. This becomes particularly evident when applying regional climate models (RCMs) at convection permitting and nonconvection permitting model resolution; *Hohenegger et al*. [2009] show that the sign of soil moisture-precipitation feedback depends also on the convection parameterization.

Land-atmosphere coupling is also important in the context of climate change. With the expected change in large-scale precipitation regimes as projected by global climate models (GCMs, see Intergovernmental Panel on Climate Change Fifth Assessment Report [*Stocker et al*., 2013]), land-atmosphere interactions are also expected to change and lead to a shift in the transition zones between weak and strong coupling regimes [*Seneviratne et al*., 2006; *Dirmeyer et al*., 2014].

The regional details of such shifts can be assessed with RCMs owing to their more detailed representation of surface heterogeneities and atmospheric processes [*Flato et al*., 2013]. In the last decade, community efforts in RCM modeling have been organized in projects PRUDENCE (Prediction of Regional scenarios and Uncertainties for Defining EuropeaN Climate change risks and Effects) [*Christensen and Christensen*, 2007] and ENSEMBLES (Ensembles-Based Predictions of Climate Changes and Their Impacts) [*Van der Linden and Mitchell*, 2009] for the European domain. Due to their common experiment design, the model ensembles allow for an assessment of uncertainties in both present and projected future climate as well as providing a basis for model intercomparisons, evaluations, and improvements. The Coordinated Regional Climate Downscaling Experiment (CORDEX) is the latest of these coordinated RCM experiments and provides an unprecedented ensemble of state-of-the-art RCMs downscaling the Coupled Model Intercomparison Project Phase 5 (CMIP5) global model results for different regions worldwide [*Giorgi et al*., 2009].

For the European domain (EURO-CORDEX) several joint evaluation studies have been performed based on ERA-Interim reanalysis-driven RCM simulations. *Kotlarski et al*. [2014] evaluated mean temperature and precipitation in the EURO-CORDEX evaluation ensemble from 1989 to 2008 and reported slight improvements compared to the ENSEMBLES simulations. In a study by *Vautard et al*. [2013] EURO-CORDEX participating RCMs showed an overall satisfying performance in the reproduction of heat waves, albeit accompanied by a large ensemble spread. Both studies highlighted the strong influence of RCM parameterizations on the model results. Applying the WRF RCM in Germany, *Milovac et al*. [2016] showed that the choice of the planetary boundary layer parameterization and the land surface model both impact simulated land-atmosphere coupling and affect the whole atmospheric boundary layer. *Bachner et al*. [2008] report a strong impact of 12 different sets of parameterizations in the RCM COSMO-CLM on precipitation over Germany for 11 summer seasons; the inferred model uncertainty range for extreme precipitation indices ranged between 20 and 50%. *García-Díez* [2014] found that a multiphysics ensemble of the WRF RCM can produce a similar spread as a multimodel ensemble within EURO-CORDEX, and *García-Díez et al*. [2015] confirm that no parameterization combination performs best for all applications. While some causalities for the differences in model results are shown, e.g., *Vautard et al*. [2013] point out sensitivity of very high near-surface air temperatures to

microphysics and convection schemes, these studies recommend extended evaluation efforts for different model components and variables. For the subset of WRF simulations within the EURO-CORDEX ensemble *Katragkou et al*. [2015] evaluated shortwave and longwave radiation and cloud cover and their relation to temperature and precipitation biases. In an evaluation study on the added value of increased spatial resolution on the reproduction of precipitation extremes, *Prein et al*. [2015] provide evidence that the high-resolution 12 km simulations for the EURO-CORDEX model domain reproduce mean and extreme precipitation better than their coarser (50 km) counterparts. *Casanueva et al*. [2015] also show the added value of the high-resolution simulations regarding the spatial precipitation patterns.

Greve et al. [2013] evaluated the root zone soil moisture exemplarily for a WRF simulation on the EURO-CORDEX domain (see model version WRF-331H in Table 1); they show the capability of WRFs land surface model (LSM) NOAH to correctly simulate soil water content in croplands and also highlight the necessity of high-quality vegetation and soil texture maps. They also found that the annual cycle explains approximately 60% of the soil moisture variability. Furthermore, all seasons show an intraseasonal variability being strongest in summer. The general circulation variability expressed in terms of the North Atlantic Oscillation explains only some of the intraseasonal variability and highlight the need to study the role of soil water content in land-atmosphere coupling in climate studies.

As part of the joint EURO-CORDEX analysis efforts, this study investigates the land-atmosphere coupling in a subset of 16 RCM simulations from the EURO-CORDEX reanalysis-driven ensemble. Many of the RCM simulation differences referred to above can be either directly or indirectly related to the reproduction of the land-atmosphere coupling in these models. The focus of the present study is on soil moisture-temperature feedbacks during the summer months of June, July, and August, when the land-atmosphere coupling is most relevant.

We particularly evaluate the reanalysis-driven simulations with respect to soil moisture, latent and sensible heat flux, which have not been analyzed in previous EURO-CORDEX evaluation analyses. An adequate reproduction of these variables is mandatory for a realistic coupling strength simulation. Two simple coupling strength metrics are then applied to the simulations, which highlight the differences in the coupling regimes and transition zones. This information can act as a baseline for the assessment of land-atmosphere coupling changes in the EURO-CORDEX regional climate change projections. These metrics also help in better understanding differences between the RCM results.

The paper is structured as follows: The RCM simulations, observational data sets, and the coupling metric are introduced in section 2. In section 3, model output for soil moisture and surface fluxes is compared to a satellite-based root zone soil moisture data set and with turbulent heat fluxes derived from FLUXNET flux tower measurements. The analysis of land-atmosphere coupling based on the correlation of the simulated surface sensible and latent heat fluxes as well as latent heat flux and air temperature, and a comparison of the results with coupling strengths derived from station observations as well as a gridded dataset follow in section 4. The results are summarized and discussed in section 5.

2. Data and Methods

2.1. EURO-CORDEX RCM Simulations

The land-atmosphere coupling analysis is based on parts of the EURO-CORDEX evaluation ensemble simulations [*Kotlarski et al*., 2014] which cover the time span from 1989 to 2008. To allow for model spin-up, only data from 1990 onward were used. The EURO-CORDEX focus domain is shown in Figure 1. The RCMs are driven by ERA-Interim reanalysis data at 0.75° resolution [*Dee et al*., 2011]. Thus, the EURO-CORDEX simulations follow the observed large-scale weather conditions and can be compared with observations also on significantly smaller than climatological time scales. Our analysis is performed with the output of 16 RCMs including 8 different WRF simulations as a subset of the EURO-CORDEX evaluation ensemble. Thirteen simulations were performed with 0.44° (EUR-44) and three with 0.11° (EUR-11) grid spacing. Table 1 contains an overview of the simulations used in this study; each RCM is identified by a unique abbreviation throughout the study. All WRF simulations use the land surface model (LSM) NOAH and the boundary layer scheme YSU [*Hong et al*., 2006], but different combinations of other atmospheric parametrization schemes. For a detailed description of the different model setups we refer to *Vautard et al*. [2013] and *Katragkou et al*. [2015]. In addition to these main

Journal of Geophysical Research: Atmospheres
10.1002/2016JD025476

Table 1. EURO-CORDEX Model Simulations Used in This Study[a]

Model ID (Resolution), ID in plots	Institute	Radiation Scheme	Convection Scheme	Microphysics Scheme	Boundary Layer Scheme	Land Surface Model	Land Use	Assessed in
ALADIN (0.44°), HMS-ALADIN	HMS	*Mlawer et al.* [1997] and *Fouquart and Bonnel* [1980]	*Cuxart et al.* [2000] and *Bougeault* [1985]	*Smith* [1990] and *Ricard and Royer* [1993]	*Troen and Mahrt* [1986]	SURFEX: *Masson et al.* [2013]	ECOCLIMAP: *Champeaux et al.* [2005] and *Masson et al.* [2003]	
CLM (0.44°), CLM-CCLM	CCLM	*Ritter and Geleyn* [1992]	*Tiedtke* [1989]	*Doms et al.* [2011] and *Baldauf and Schulz* [2004]	*Louis* [1979]	TERRA-ML: *Doms et al.* [2011]	Joint Research Centre: Global land cover 2000 database [2003]	Ko, V
HadRM3P (0.44°), MOHC-HadRM3P	MOHC	*Edwards and Slingo* [1995]	*Gregory and Rowntree* [1990] and *Gregory et al.* [1997]	*Smith* [1990] and *Martin et al.* [1994]	*Smith* [1990]	*Essery et al.* [2003]	*Hansen et al.* [2000]	*Massey et al.* [2015]
HIRHAM (0.44°), DMI-HIRHAM	DMI	*Morcrette et al.* [1986]	*Tiedtke* [1989]	*Lohmann and Roeckner* [1996]	*Louis* [1979]	*Hagemann* [2002]	*Claussen et al.* [1994]	Ko
RACMO2 (0.44°), KNMI-RACMO	KNMI	*Fouquart and Bonnel* [1980]	*Tiedtke* [1989], *Nordeng* [1994] and *Neggers et al.* [2009]	*Tiedtke* [1993] and *Tompkins et al.* [2007], ECMWF-IFS: *Neggers* [2009]	*Lenderink and Holtslag* [2004] and *Siebesma et al.* [2007]	*Van Den Hurk and Viterbo* [2000] and *Balsamo et al.* [2009]	ECOCLIMAP: *Champeaux et al.* [2005] and *Masson et al.* [2003]	Ko, V
RACMO2 (0.11°), KNMI-RACMO11	KNMI	Same as 0.44°	Same as 0.44°	Same as 0.44°	Same as 0.44°	Same as 0.44°	Same as 0.44°	Ko, V
RCA4 (0.44°), SMHI-RCA	SMHI	*Savijärvi* [1990]	*Kain and Fritsch* [1993]	*Rasch and Kristjánsson* [1998]	*Cuxart et al.* [2000]	*Samuelsson et al.* [2006]	ECOCLIMAP: *Champeaux et al.* [2005] and *Masson et al.* [2003]	Ko, V
REMO 2009 (0.44°), GERICS-REMO	GERICS	*Morcrette et al.* [1986]	*Tiedtke* [1989]	*Lohmann and Roeckner* [1996]	*Louis* [1979]	*Hagemann* [2002] and *Rechid et al.* [2009]	USGS: *Hagemann* [2002]	Ko, V
WRF-331A (0.44°), MIUB-WRF	MIUB	CAM3: *Collins et al.* [2004]	Modified Kain-Fritsch: *Kain* [2004]	WSM 6-class: *Hong and Lim* [2006]	YSU: *Hong et al.* [2006]	NOAH: *Ek et al.* [2003]	IGBP-MODIS 30″	Ka, Ko, V
WRF-331A2 (0.44°), AUTH-WRF	AUTH	CAM3: *Collins et al.* [2004]	Modified Kain-Fritsch: *Kain* [2004]	WSM 6-class: *Hong and Lim* [2006]	YSU: *Hong et al.* [2006]	NOAH: *Ek et al.* [2003]	IGBP-MODIS 30″	Ka, V
WRF-331C (0.44°), BCCR-WRF	BCCR	CAM3: *Collins et al.* [2004]	Modified Kain-Fritsch: *Kain* [2004]	WSM 3-class: *Hong et al.* [2004]	YSU: *Hong et al.* [2006]	NOAH: *Ek et al.* [2003]	IGBP-MODIS 30″	Ka, V
WRF-331D (0.44°), IDL-WRF	IDL	RRTMG: *Iacono et al.* [2008]	Betts-Miller-Janjic: *Janjić* [1994]	WSM 6-class: *Hong and Lim* [2006]	YSU: *Hong et al.* [2006]	NOAH: *Ek et al.* [2003]	IGBP-MODIS 30″	Ka
WRF-331 F (0.11°), IPSL-WRF11	IPSL-INERIS	RRTMG: *Iacono et al.* [2008]	*Grell and Dévényi* [2002]	WSM 5-class: *Hong et al.* [2004]	YSU: *Hong et al.* [2006]	NOAH: *Ek et al.* [2003]	USGS land use	Ka, Ko, V
WRF-331G (0.44°), UCAN-WRF	UCAN	CAM3.: *Collins et al.* [2004]	*Grell and Dévényi* [2002]	WSM 6-class: *Hong and Lim* [2006]	YSU: *Hong et al.* [2006]	NOAH: *Ek et al.* [2003]	IGBP-MODIS 30″	Ka, V
WRF-331H (0.11°), UHOH-WRF11	UHOH	CAM3: *Collins et al.* [2004]	Modified Kain-Fritsch: *Kain* [2004]	Morrison 2-mom. scheme: *Morrison et al.* [2009]	YSU: *Hong et al.* [2006]	NOAH: *Ek et al.* [2003]	IGBP-MODIS 30″	Ko, V
WRF-341E (0.44°), NUIM-WRF	NUIM	RRTMG: *Iacono et al.* [2008]	Modified Kain-Fritsch: *Kain* [2004]	WSM 6-class: *Hong and Lim* [2006]	YSU: *Hong et al.* [2006]	NOAH: *Ek et al.* [2003]	IGBP-MODIS 30″	

[a]The RCMs are identified throughout the study with the model and institute IDs. For further details of the model configuration and parameterization see *Katragkou et al.* [2015, Table 1] (Ka), *Kotlarski et al.* [2014, Table 1] (Ko), and *Vautard et al.* [2013, Table 1] (V).

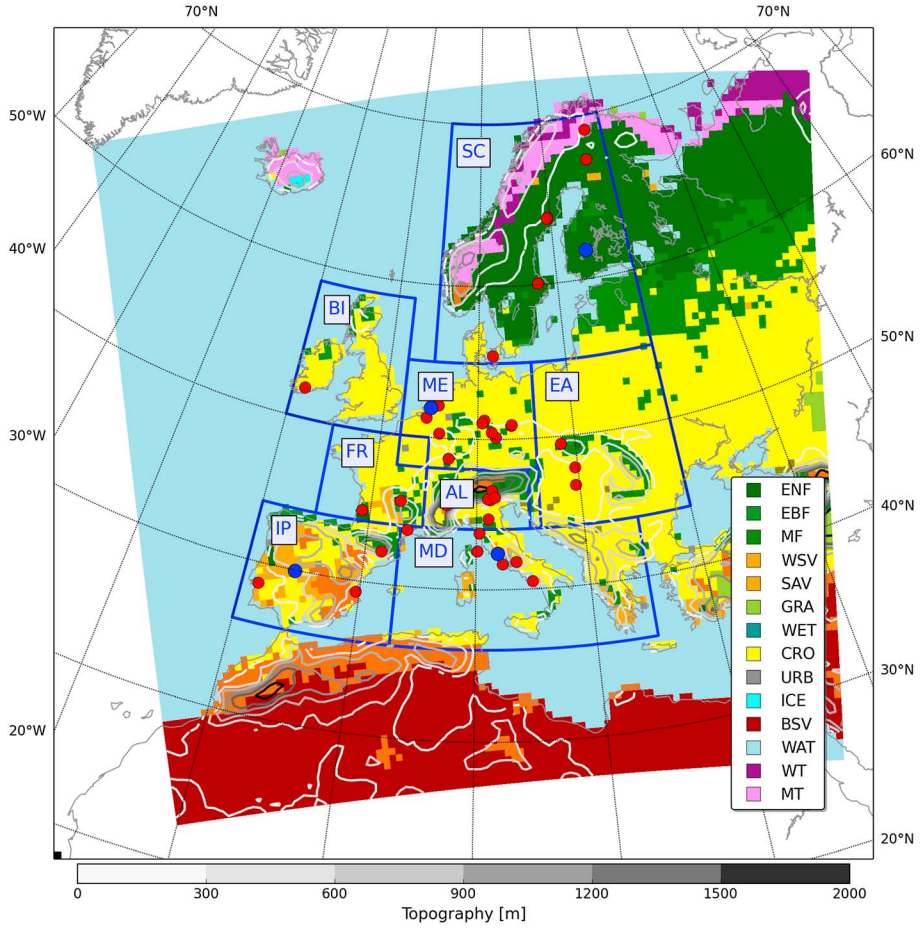

Figure 1. EURO-CORDEX EUR-44 and EUR-11 domain. Colors indicate as an example the dominant land use types derived from the Moderate Resolution Imaging Spectroradiometer (MODIS) satellite data classification used in the WRF models, while gray isolines indicate topography (ENF: evergreen needleleaf forest; EBF: evergreen broadleaf forest; MF: mixed forest; WSV: wooded savanna; SAV: savanna; GRA: grasslands; WET: wetlands; CRO: cropland; URB: urban; ICE: snow or ice; BSV: barely/sparsely vegetated; WAT: water; WT: wooded tundra; MT: mixed tundra). The blue boxes delineate the PRUDENCE analysis regions with their identifiers, and dots show the locations of the FLUXNET stations (red: all stations used in the study; blue: stations shown in section 3.2).

settings, the models also differ, e.g., in the configuration of the lateral boundary relaxation zone around the EURO-CORDEX focus domain, the number of vertical levels, or interpolation settings for initial and static fields. These configurations can lead to larger ensemble spreads than for pure multiphysics ensembles [*García-Díez et al.*, 2015]. Thus, the ensemble analyzed is an "ensemble of opportunity," which merely collects all simulations providing the required fields for the analysis. This also implies some inevitable restrictions when not all desirable parameters for this study were stored, such as upper soil moisture.

2.2. Observational Data Sets

2.2.1. Global Land Evaporation Amsterdam Model

For the evaluation of soil moisture and latent heat flux as well as the coupling metric calculated from the correlation of latent heat flux and 2 m temperature (introduced in the next subsection) we use the Global Land Evaporation Amsterdam Model (GLEAM) data set version v3a [*Martens et al.*, 2016]. It provides terrestrial evaporation and root zone soil moisture based on satellite-observed soil moisture through data assimilation of European Space Agency Climate Change Initiative soil moisture (ESA CCI SM) [*Liu et al.*, 2011a; *Wagner et al.*, 2012], vegetation optical depth [*Liu et al.*, 2011b], and snow water equivalents [*Armstrong et al.*, 2005], ERA-Interim reanalysis air temperature and radiation, and the Multi-Source Weighted-Ensemble Precipitation (MSWEP) product [*Beck et al.*, 2016]. The daily data are provided on a global 0.25° × 0.25° grid

and covers the period from 1980 to 2014. To ease the comparisons between the simulated and GLEAM data both data are projected on to a rotated 0.22° × 0.22° latitude-longitude grid by nearest neighbor resampling. This grid has the same rotated pole (198.0; 39.25) as the EURO-CORDEX domain. For comparison with EUR-44 simulation data, the four points of the 0.22° grid fitting into one EUR-44 grid cell are averaged. For the EUR-11 simulation data, a four point RCM average is compared with the 0.22° grid GLEAM data. Only grid points defined as land points in both the RCM's and the satellite data's land masks are considered.

2.2.2. FLUXNET

Simulated latent and sensible heat fluxes are compared with the European FLUXNET observations [*Baldocchi et al*., 2001; www.fluxdata.org, and references therein]. This data product contains preprocessed, quality-checked, and instrument error-corrected observations from eddy covariance flux tower stations operated over central Europe with a highly variable data coverage from 1996 to 2007. We compare FLUXNET point observations with RCM time series from the closest grid point. Only days for which all half-hourly values have a quality flag 0 or 1 (representing original or high-quality gap-filled data) and only months with a minimum of 20 high-quality days are taken into account. In total 42 stations meet these criteria with at least 3 years of high-quality data each; see Figures 1 and 9 for their geographic location. Since the simulations are driven by reanalysis data only at the lateral boundaries, the simulated weather conditions inside the RCM model domain on local and daily scales may differ considerably from the actual weather experienced at the FLUXNET stations. Hence, mean seasonal cycles are compared similar to, e.g., *Jaeger et al*. [2009] and shown for four representative stations from contrasting climate regions and different vegetation types: Cabauw (Netherlands), Las Majadas (Spain), Hyytiala (Finland), and Roccarespampani (Italy).

For the interpretation of the comparison it is important to note that eddy covariance flux tower measurements can be systematically too low and that the energy balance is often not closed [*Stoy et al*., 2013; *Wizemann et al*., 2015]. In order to assess this systematic error, a comparison of all energy balance components including ground heat flux and net radiation is needed. Under the assumption that the radiation measurement errors are much smaller than the turbulent flux measurement errors, the net radiation is considered as a reference and the systematic underestimation of the observed heat fluxes is estimated to range from 0% to 40% for each of the 42 stations. For all but one station, the sum of the three surface fluxes is 30% to 35% lower than the net radiation. Analogous to *Jaeger et al*. [2009], the residual is assumed to be caused by equally underestimated turbulent fluxes and thus added to the latent and sensible heat flux following the Bowen ratio. In reality, however, the residual depends on terrain, surface properties, and the condition of the atmospheric boundary layer, and thus, a correct Bowen ratio is just an assumption [*Ingwersen et al*., 2011; *Wizemann et al*., 2015].

2.3. Land-Atmosphere Coupling Metric

The correlation between two characteristic variables connected to surface exchange processes, such as air temperature correlated to latent heat flux or net radiation correlated to latent heat flux, is considered as a useful land-atmosphere coupling metric [*Seneviratne et al*., 2010]. Such a coupling metric addresses in particular the soil-moisture-temperature feedback process, the focus of the present study. Other than coupling metrics that are based on special experiment designs, e.g., the GLACE-type coupling measures [*Koster et al*., 2006; *Seneviratne et al*., 2006], this correlation-based metric can be applied to standard RCM output variables and is thereby also suitable for the intercomparison of an arbitrary RCM ensemble.

Another coupling metric is the correlation between the sensible heat (*H*) and latent heat flux (LE) as both variables are the components of the surface energy balance, which compete for the redistribution of net surface radiation energy into other energy forms. For energy-limited regions soil moisture is available in sufficient amounts. In this case, land surface temperature also dictates near-surface atmospheric humidity resulting in concordant near-surface moisture and temperature gradients and a positive correlation between both fluxes. For water-limited regions, however, soil moisture limits evapotranspiration—and thus also near-surface atmospheric humidity and its gradient—while temperature gradients and sensible heat fluxes may still increase in response to increasing radiation. Since latent heat fluxes in turn further reduce soil moisture, correlations between the two fluxes become smaller or even negative. In this case even small changes in soil moisture affect the near-surface atmosphere profoundly. Figure 2 shows exemplarily the *H*-LE correlation based on daily mean values for the June–August (JJA) summer seasons in 2002 and 2003 for the MIUB-WRF simulation. Contrasting patterns appear for central and western Europe: In 2003 negative correlations

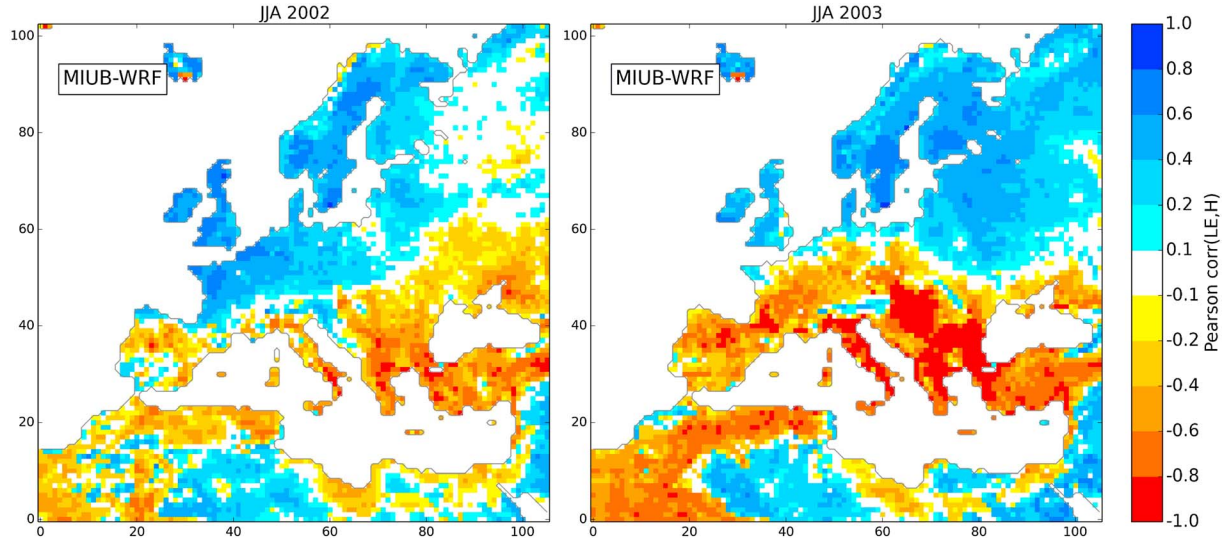

Figure 2. Correlation of daily mean latent and sensible heat flux for summer (JJA) (left) 2002 and (right) 2003 based on the MIUB WRF EUR-44 simulation.

indicate strong coupling related to anomalous warm and dry conditions, which culminated in the well-known western European heat wave in August. In contrast, the summer season of 2002 is characterized by rather wet conditions giving rise to positive turbulent flux correlations in this region. Regarding the noisy pattern in Northern Africa, please note that the *H*-LE (as well as the LE-*T*) correlation-based metric is only meaningful in regions where evapotranspiration is reasonably large [*Seneviratne et al*., 2006].

Within this study, in the coupling analysis in section 4, the intercomparison of the RCM ensemble is first based on *H*-LE correlations calculated from 10 day mean values over the summer seasons of the full period 1990–2008. This *H*-LE correlation is the diagnostic we use to access coupling strengths in comparison to the FLUXNET station data. Furthermore, the correlation of evaporative fraction (LE/*H* + LE) and total soil moisture is used in section 4 for the RCM intercomparison of the link between soil moisture and flux partitioning. A further coupling metric we use is the correlation of latent heat flux (LE) and 2 m air temperature (*T*) based on 10 daily mean summer (JJA) values of the period from 1990 to 2008. For evaluation of the RCM results the metric is also calculated from the GLEAM evaporation and ERA-Interim 2 m air temperature. Using ERA-Interim air temperatures seems most suitable since these temperature data are also used as forcing data for GLEAM. While both metrics describe the soil moisture-temperature coupling process, the *H*-LE correlation indicates the process of changing flux partitioning at the surface, the LE-*T* correlation describes the second step of the feedback pathway into the atmosphere.

It is important to note that there is no unique way to define land-atmosphere coupling strength, and since different metrics address individual processes in the complex land-atmosphere feedback system, they can show different results. Also, a direct comparison of different coupling metrics is hampered since the value ranges and units differ and the definition of "strong" and "weak" may not be consistent. *Lorenz et al*. [2015] suggest that specific coupling experiments like GLACE are required to scale the different measures for each particular climate model.

3. Model Evaluation

3.1. Soil Moisture

The different LSMs in the RCMs analyzed have very different soil characteristics; thus, a direct comparison of the available total (i.e., vertically integrated) soil moisture is not meaningful. Especially, the differing depths of the soil layers and the saturation levels related to soil porosity make a grid pointwise comparison of the total soil moisture amounts of the individual models difficult. Despite exhibiting different mean total soil moisture amounts, the RCMs are expected to reproduce typical intra-annual as well as interannual variability for different regions in Europe.

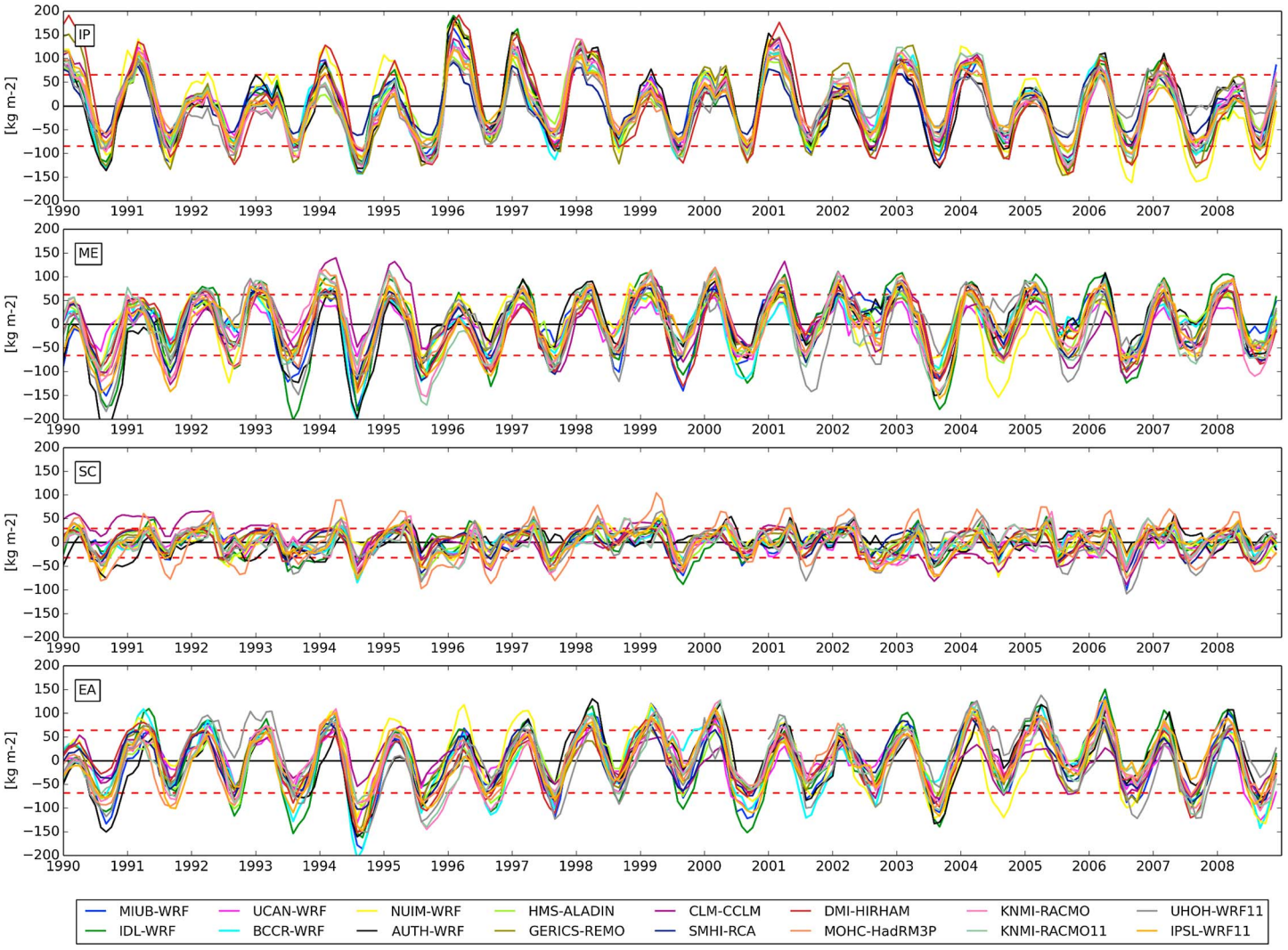

Figure 3. Time series of total (vertically integrated) soil moisture anomalies (individual RCM mean 1990–2008 subtracted) averaged for PRUDENCE regions Iberian Peninsula, middle Europe, Scandinavia, and eastern Europe. Red dashed lines indicate the ensemble mean annual minimum and maximum values averaged for the whole time span.

Figure 3 shows time series of monthly total soil moisture anomalies where the individual RCM's long-term mean has been subtracted. Spatial averages for different PRUDENCE regions are plotted for the Iberian Peninsula, middle Europe, Scandinavia, and eastern Europe. Though the different soil characteristics still affect the potential maximum dynamic range (minimum minus maximum) of the models, the figure allows for a comparison of the annual cycle and representation of wet and dry anomalies in individual years. For all regions all RCMs' soil moisture time series show a clear annual cycle. The average maximum soil moisture is reached in March and the minimum in September with overall agreement between the RCMs and slight interannual variability in timing. In the southern European regions the minimum is reached a few weeks later. The mean range between yearly minimum and maximum multimodel mean (indicated by the red dashed lines) is dependent on the soil characteristics and the climate conditions.

With a precipitation maximum during winter and high demand for evapotranspiration during the dry summer months, the Iberian Peninsula shows the largest mean range with 140 kg m^{-2}, compared to also well-pronounced amplitudes of 120 kg m^{-2} and 110 kg m^{-2} in eastern and central Europe. In Scandinavia the range is much smaller, the annual cycle is less pronounced, and the individual RCM simulations are less correlated to each other when the annual cycle is removed. The weaker annual cycle is related to overall wet conditions throughout the year and a smaller amount of evapotranspiration in this energy-limited high-

latitude region. Here the differences in the annual cycle between the RCMs most likely result from effects of snow cover and frozen soils. For all regions a distinct interannual variability is evident, both for the maxima and minima as well as for the seasons in between. The variability of the minima is larger than the maxima in those regions where the winter is wet enough to reach near-saturation conditions frequently, as seen, e.g., in central Europe (standard deviation of ensemble mean yearly minima is 24.1 $kg\,m^{-2}$ versus 14.8 $kg\,m^{-2}$ for the maxima). For the Iberian Peninsula also soil moisture maxima during winter show a larger interannual variability (here the standard deviation of the minima is 13.9 $kg\,m^{-2}$ versus 32.3 $kg\,m^{-2}$ of the maxima). Despite some outliers for some models and years, the RCMs show overall good agreement in simulating the soil moisture differences between individual years; anomalously wet and dry seasons are captured quite consistently, e.g., the wet conditions during the summer 2002 in central Europe and the very dry summer in 2003 or the wet year 1996 in the Iberian Peninsula region.

So far the RCMs intra-annual and interannual variations in vertically integrated total soil moisture have been intercompared among each other. In the following, we investigate the RCMs' ability to reproduce the GLEAM soil moisture (with assimilated ESA CCI satellite-based soil moisture) patterns for Europe. We restrict the comparison of the RCMs total soil moisture to the GLEAM root zone soil moisture to the correlation of summertime monthly means for JJA over the period from 1990 to 2008, which is shown in Figure 4. Since the soil moisture typically follows an annual cycle that per se leads to a positive correlation, consequently the individual RCM's mean annual cycle is subtracted so that the correlation is based on monthly anomalies from the individual long-term monthly means. Overall, the RCMs show significant positive correlation with the GLEAM soil moisture for large parts of Europe. Except for the pluvious Moroccan-Algerian Atlas region, there is no significant correlation for Northern Africa due to the very dry summer conditions and hence small soil moisture variations. The comparison shows regional differences for the individual RCMs correlation to GLEAM soil moisture. While in some regions, e.g., the Iberian Peninsula and the British Isles, a positive correlation prevails, in other regions, e.g., Poland and Ukraine, the RCMs predominantly do not show a significant correlation with GLEAM. Although RCMs like KNMI-RACMO, HMS-ALADIN, and IPSL-WRF have larger areas of positive correlation with the GLEAM soil moisture, no single RCM is outperforming the others across the domain. Despite the fact that the WRF RCMs feature the same LSM, there is no WRF-specific soil moisture pattern. For example, the MIUB-WRF and IDL-WRF simulations show a high correlation in southeastern Europe, while the NIUM-WRF and AUTH-WRF simulation are not significantly correlated with the GLEAM soil moisture in this region. For northeastern Europe the KNMI-RACMO simulations show the largest agreement with the GLEAM data. Comparing both resolutions (EUR-44 and EUR-11), the large-scale pattern is similar; differences remain on the local scale. When all months of the other seasons are taken into account the patterns are similar whereby the correlation is generally slightly higher (data not shown).

In general, areas of uncorrelated RCM to GLEAM soil moisture may exist for multiple reasons, both from the models and data point of view: differences in soil and vegetation parameterization, unrepresented lateral soil moisture flow and irrigation, and internal variability of weather patterns in the individual RCM runs. The latter may explain the higher correlations in western parts of Europe, where the weather patterns possibly agree better and the internal variability is smaller due to the closer distance to the western lateral boundary and prevailing westerlies. This would need some further investigation.

Unfortunately it is not possible to directly intercompare absolute values of total soil moisture or to determine biases for the different RCM's LSMs. In different models (and also for same models but different soil texture and vegetation type) the same amounts of soil moisture may be an indication of energy-limited conditions in one and soil moisture-limited conditions in another model. The impact on the flux partitioning, however, is decisive for the coupling to the atmosphere, which will be investigated in the following sections. To this point the RCMs have shown a reasonably well reproduction of the 1990–2008 soil moisture interannual and intraseasonal variability.

3.2. Surface Fluxes

The following section investigates the RCMs representation of both latent and sensible heat flux. Figure 5 compares the mean seasonal cycles of latent and sensible heat flux simulated by the 16-member EURO-CORDEX ensemble for four FLUXNET stations representative for different climate. Both data sets are averaged over the subset of years for which high-quality FLUXNET data are available.

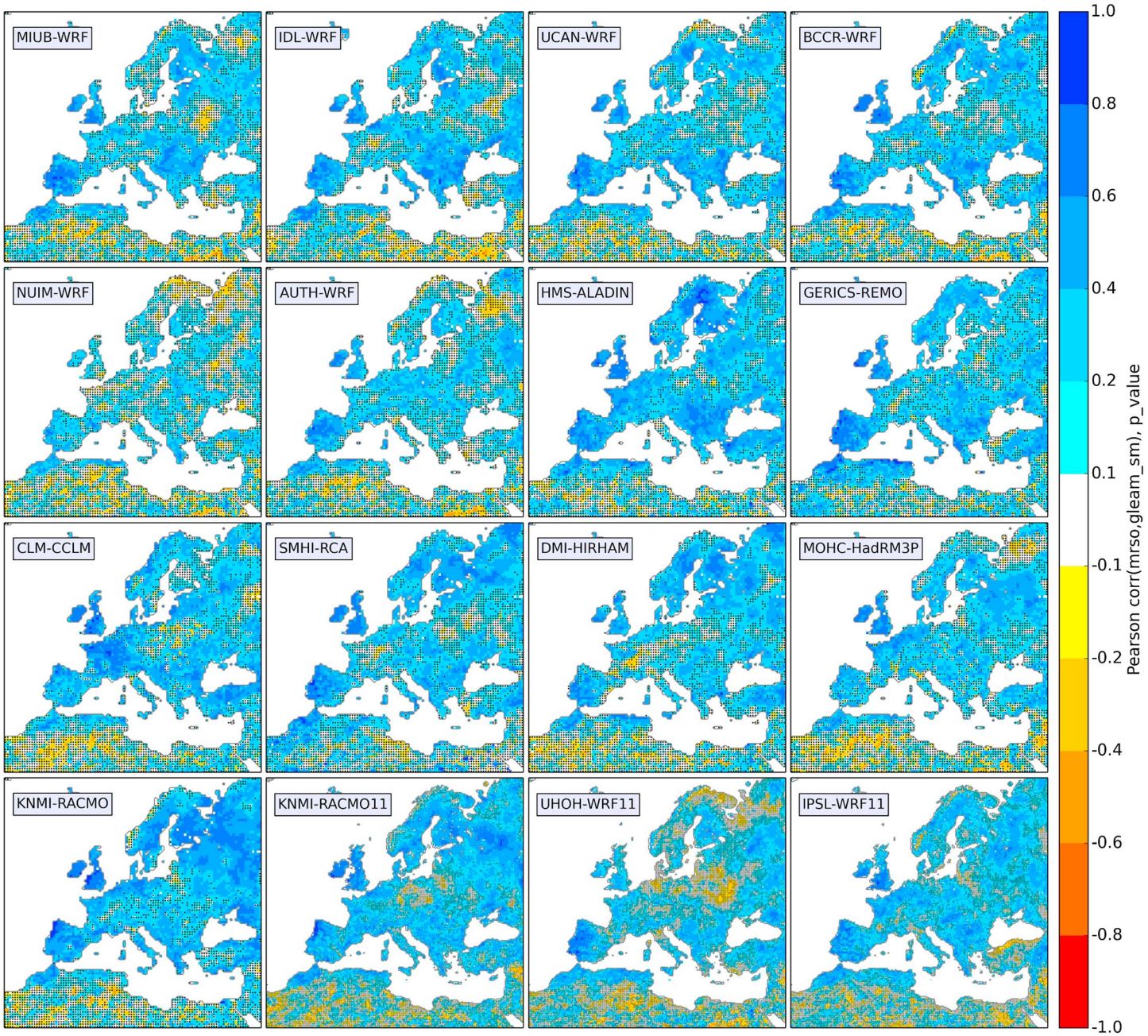

Figure 4. Correlation of GLEAM volumetric near-root zone soil moisture and vertically integrated total soil moisture in individual RCM simulations (monthly means subtracted by individual RCM's long-term monthly means, JJA, 1990 to 2008, dotted where correlation is below 5% significance level).

The typical soil moisture-related partitioning between latent and sensible heat as captured by the FLUXNET observations is reproduced by the RCM ensemble. For example, in the Netherlands, where conditions with high soil moisture prevail, latent heat fluxes on average exceed sensible heat fluxes, whereas in Spain the sensible heat flux dominates in summer due to soil moisture limitation while latent heat flux is highest in spring. Individual model simulations, however, may differ substantially from the FLUXNET observations and show larger differences for some locations (see, e.g., the comparison at station IT-Ro1). Such differences can be related to different land use types at the station and in the model, which stresses the sensitivity of flux partitioning to surface characteristics. Model runs at the higher EUR-11 resolution better represent surface heterogeneities, but the 12 km × 12 km grid cells are still much larger than the typical footprint of a flux tower station. Moreover, even results from individual model runs with exactly the same surface type differ owing to

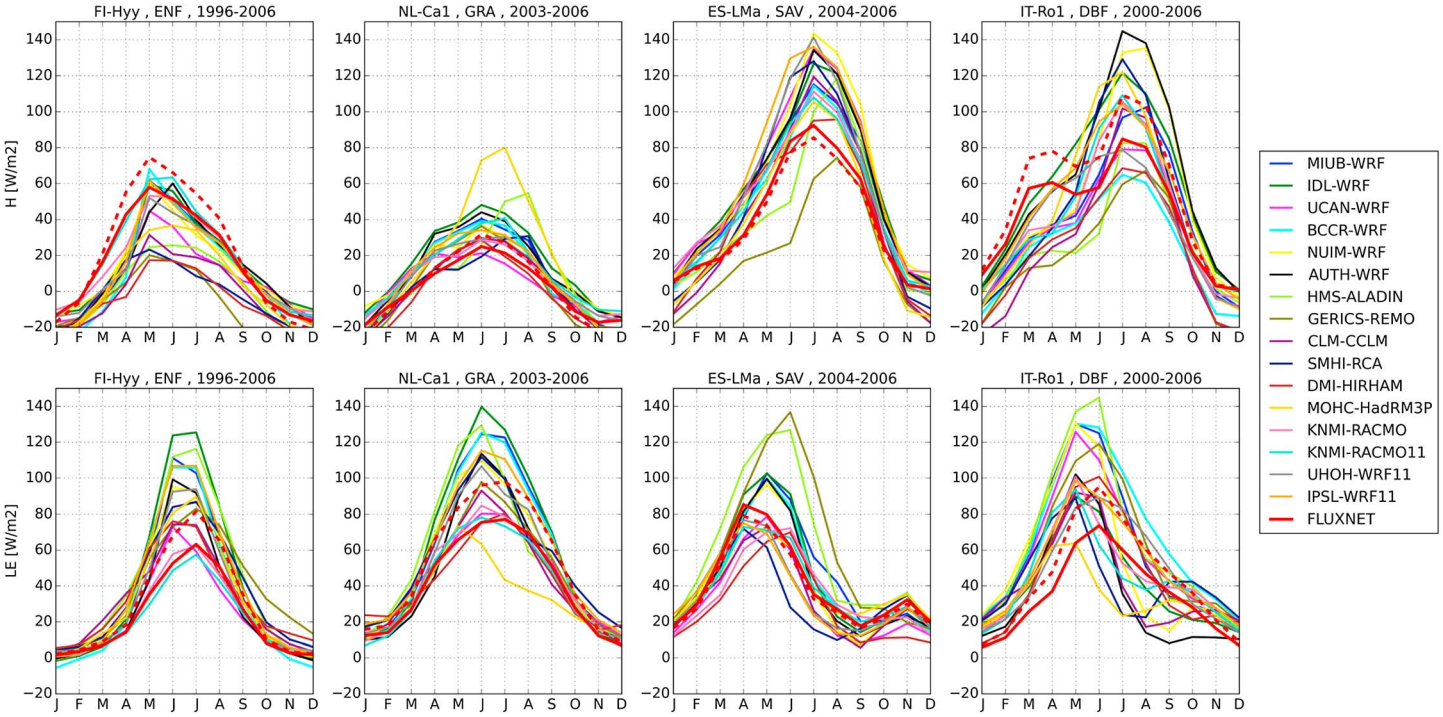

Figure 5. Mean annual cycles of monthly mean of (top row) sensible and (bottom row) latent heat flux at four representative FLUXNET stations (thick red line) and derived from the closest model grid points. The red dashed line indicates an estimated correction of the flux tower measurement bias by adding the residual of the energy balance according to the Bowen ratio (assuming net radiation and ground heat flux to be correct). Only years with high-quality FLUXNET data are included. Stations from left to right are Hyytiala (Finland) with evergreen needleleaf forest (years 1997–2006), Cabauw (Netherlands) with grassland (years 2003–2006), Las Majadas (Spain) with savanna (years 2004–2006), and Roccarespampani-1 (Italy) with deciduous broadleaf forest (years 2000–2006).

differences in atmospheric conditions that may evolve in response to internal model variability, especially in net radiation and soil moisture, a key variable for flux partitioning. Despite these limitations, the FLUXNET data product is the only data set that allows for such a direct evaluation of the model fluxes.

While the expected seasonal cycle is the dominant feature, both in the observations and in the RCM simulations, the maxima produced by the individual RCMs differ substantially, e.g., up to 40–80 W m^{-2} in summer both for *H* and LE. Since the WRF RCMs use the same LSM and mostly the same surface type, the variation between the runs must be attributed to different climate states generated due to the different parameterizations.

The effects of the differences in the simulated net radiation are obvious by comparing the sum of the summertime (JJA) turbulent surface fluxes for the EURO-CORDEX domain (Figure 6). As already seen for the model grid points near FLUXNET stations (Figure 5) also this domain-wide comparison depicts systematic differences between particular RCMs. For example, the UCAN-WRF underestimates both surface heat fluxes resulting from very low net radiation, which mostly result from reduced incoming solar radiation caused by relatively high cloud cover as shown by *Katragkou et al.* [2015].

Most RCMs simulate the expected climate-related patterns in flux partitioning expressed by the mean evaporative fraction in Figure 7: dry summer climates show low evaporative fractions, e.g., in the Mediterranean region, while over wetter central and northeastern Europe latent heat fluxes exceed sensible heat fluxes.

For some regions, however, differences between the ensemble members can be large. For example, HIRHAM, RCA, and ALADIN simulate very high evaporative fractions (reaching up to 5 times higher latent than sensible heat flux) for central, northern, and eastern Europe. The different WRF simulations in turn show relatively low evaporative fractions over Scandinavia especially in the mountainous regions, which can be explained by the land cover type "barren tundra" in their common NOAH LSM and not by different climate conditions. In the WRF simulations also the grid points classified as "urban" stick out with almost zero evapotranspiration. Especially in the Mediterranean the models differ also in the spatial distribution of variability, which is most probably also a result of different land surface parametrizations. For the eight WRF model simulations the

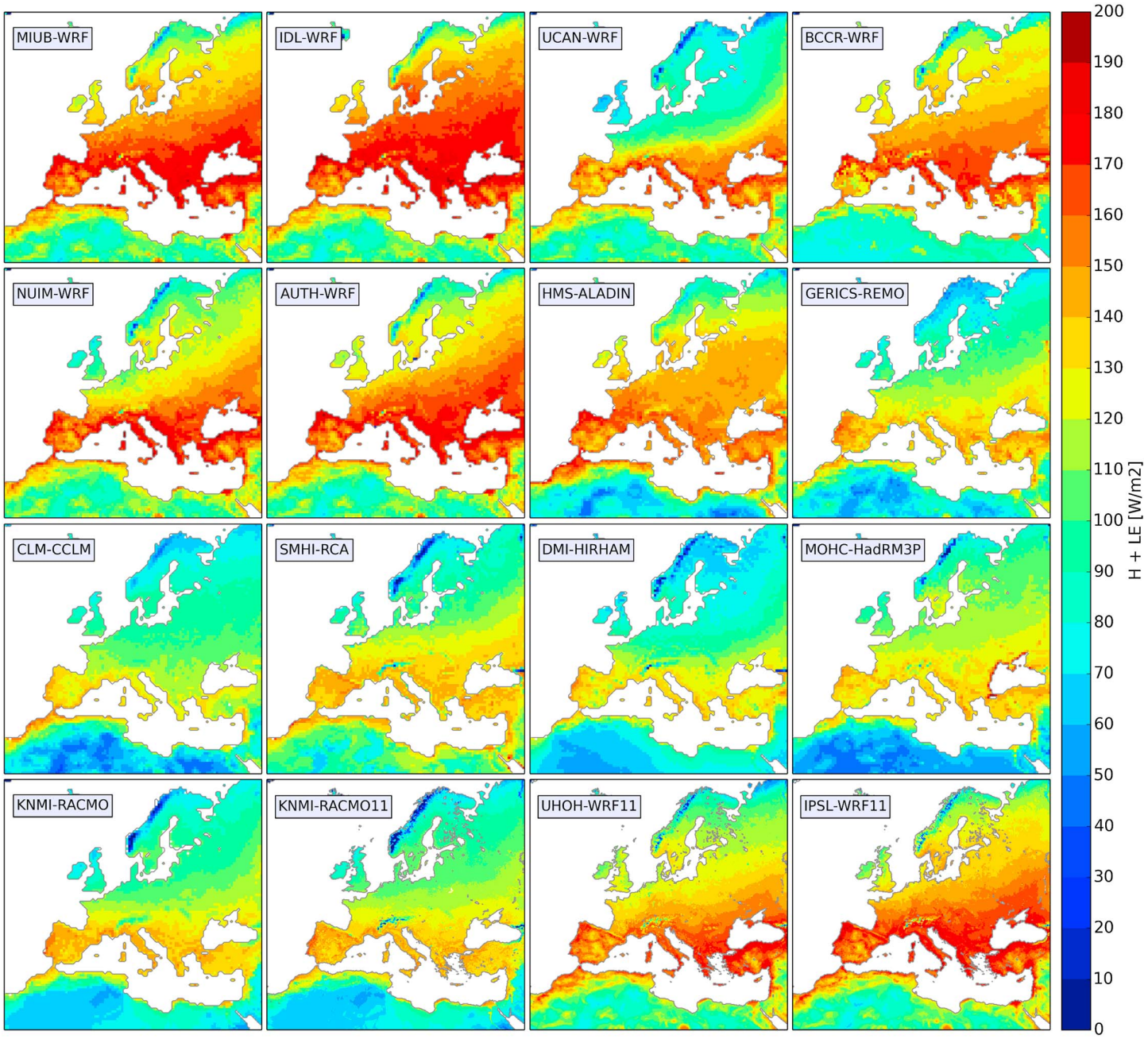

Figure 6. Spatial distribution of the summer (JJA) mean sum of latent and sensible heat flux, between 1990 and 2008. The averages were computed over the complete time span including nighttime values, which explains the comparatively low maxima.

differences only result from diverging climate conditions due to the distinctly different sets of atmospheric parameterizations, dynamics settings, or slightly different initial conditions. For these runs differences in flux partitioning are consistent with differences in near-surface soil moisture. The relatively dry conditions simulated by AUTH-WRF and NUIM-WRF for southeastern Europe contrast clearly with the wetter UHOH-WRF simulation. We will expand on the connection between soil moisture and flux partitioning in the next section.

To this point the general differences in soil moisture and surface fluxes have been assessed and linked to attendant biases in other variables such as temperature, precipitation, and radiation [*Vautard et al.*, 2013; *Kotlarski et al.*, 2014; *Katragkou et al.*, 2015]. This assessment will help to explain differences among the models when coupling strength metrics are evaluated.

4. Land-Atmosphere Coupling Analysis

4.1. EURO-CORDEX Ensemble Comparison to FLUXNET

The distinctly different seasonal cycles of latent versus sensible heat flux for different climate regions (Figure 5) suggest their correlation as an indication of coupling strength. Figure 8 shows the correlation of latent and sensible heat, our first coupling strength metric as introduced in section 2.3, for the individual RCM runs based on nonoverlapping 10 day means over the summer season (JJA) over the years 1990 to 2008.

For all RCMs weak coupling (positive correlation) prevails over northern Europe while strong coupling (negative correlation) dominates southern and southeastern Europe. This finding roughly coincides with regions attributed with strong coupling in *Seneviratne et al*. [2006], *Fischer et al*. [2007], and *Miralles et al*. [2012]. For central Europe, the location of the transition zone from one regime to the other differs considerably between some RCMs. Especially, UCAN-WRF and DMI-HIRHAM locate the transition zone farther to the south compared to the other RCMs while CLM-CCLM and HMS-ALADIN show strong coupling over a larger area which even reaches Scandinavia and Russia. For the other seasons (data not shown) coupling is much weaker than in summer. For Northern Africa the results have to be interpreted with care, since the *H*-LE correlation is not meaningful in regions with very low evapotranspiration.

On the regional scale, much of the spatial heterogeneity in coupling strength can be related to orography, respectively, its influences of more precipitation, more cloud cover and colder temperatures. The Carpathians, Alps, and Pyrenees display substantially weaker coupling strength compared to the surrounding flatter terrain.

There are a number of possible reasons for the differences in the RCM runs that cannot be clearly separated from each other. On the one hand, the different climate model states (e.g., seen in the parameters precipitation and net radiation) evolving in the individual model runs due to different atmospheric parametrizations and other settings have a major influence on the coupling strength. This influence is clearly seen for the individual WRF simulations (same LSM and PBL scheme) that show differences in mean precipitation, radiation, and temperature [*Katragkou et al*., 2015]. The relatively weak coupling produced by UCAN-WRF compared to the other WRF versions is caused by the reduced net radiation compared to the other WRF simulations. On the other hand, the individual RCM's LSM characteristics and the parametrization of the land surface (vegetation type, soil type, etc.) decisively affect the coupling strength, too. The coupling strength is thereby a useful integrative metric which may help to explain differences we observe in other parameters or phenomena. For example, if the models fail to correctly represent coupling strength, it is also highly likely that they overestimate or underestimate heat waves [*Vautard et al*., 2013]. Though this is no complete proof of causality, the intercomparison of summertime extreme temperatures (90th percentile) shows that those RCMs that show a stronger (weaker) than average coupling predominantly simulate higher (lower) than average extreme temperatures (data not shown).

We now apply the coupling analysis above to the FLUXNET observations for an evaluation of the RCMs. Figure 9 displays the correlation of 10 day averages of summertime (JJA) latent and sensible heat fluxes for several of the 42 FLUXNET stations. Only months with at least 20 days of high-quality data are used and only stations with at least 3 years of data are shown. Because measurement time periods differ for the displayed stations, differences between nearby located stations may partly result from different weather conditions during the different time periods covered. The observations show mainly negative (positive) correlations indicating strong (weak) coupling in southern (northern) parts of Europe and are thus in rough accordance with the RCM results.

A direct comparison of the 42 FLUXNET stations to the RCMs is provided in Figure 10. Here the same *H*-LE correlation values as in Figure 9 are shown, together with derived coupling strength metric from the individual RCMs. In contrast to Figure 8 the correlation from the RCMs is based on the time span for which FLUXNET observations are available. Again, a large diversity within the RCM ensemble is seen for many locations. Outliers, like the overall stronger coupling in the HMS-ALADIN run and the CLM-CCLM run for northern Europe are obvious, as well as the weaker coupling in DMI-HIRHAM, UCAN-WRF, and NUIM-WRF for most stations in central Europe. A comparison with the FLUXNET data shows that the observations are within the quantile range of the RCMs for 16 out of 42 stations. However, regarding the sign of the correlation reflecting strong or weak coupling regime, the median of the RCMs and the FLUXNET observations agree for 80% of the

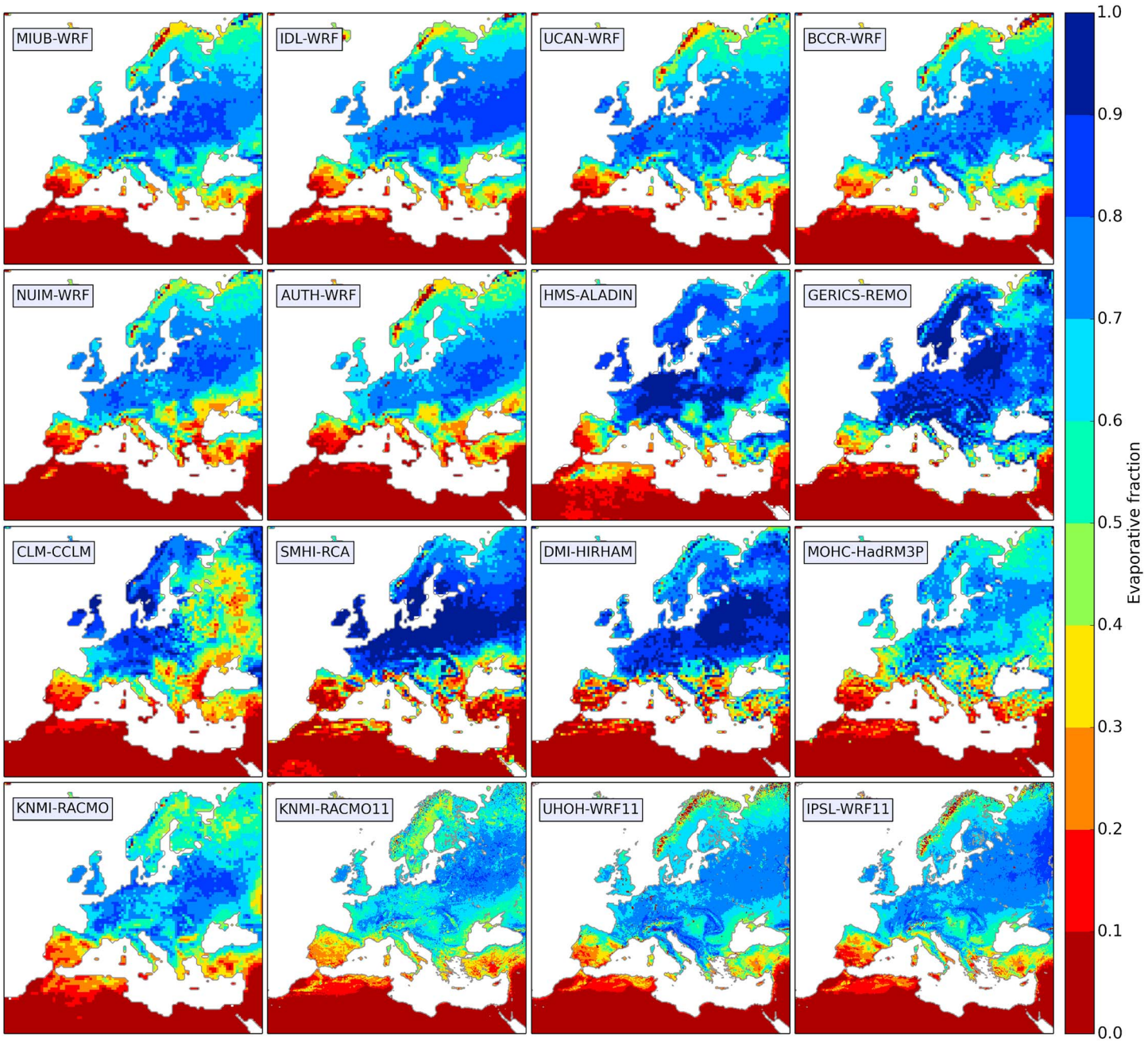

Figure 7. Summer (JJA) mean of the evaporative fraction (latent heat flux divided by the sum of latent and sensible heat flux) for the years 1990 to 2008.

stations. The number of stations where the observed *H*-LE correlation is above the 75th percentile of the RCMs (i.e., RCMs show a stronger coupling than observed) exceeds the number of stations where the RCM's coupling strength is weaker than the observed coupling strength (20 compared to 6). Also, regarding the RCM ensemble means for each station, the observed FLUXNET coupling strength in terms of *H*-LE correlations appears slightly weaker than for the RCM simulations (26 out of 42 stations).

As the stations are not equally distributed in space, it is possible that they might favor certain conditions with a similar coupling strength in locations with multiple stations and therefore reduce the representativeness of the observations. Besides variable local climate conditions, the vegetation types (indicated by the symbols in Figure 9) impact coupling strength: In the Netherland's FLUXNET stations, e.g., the correlations are higher

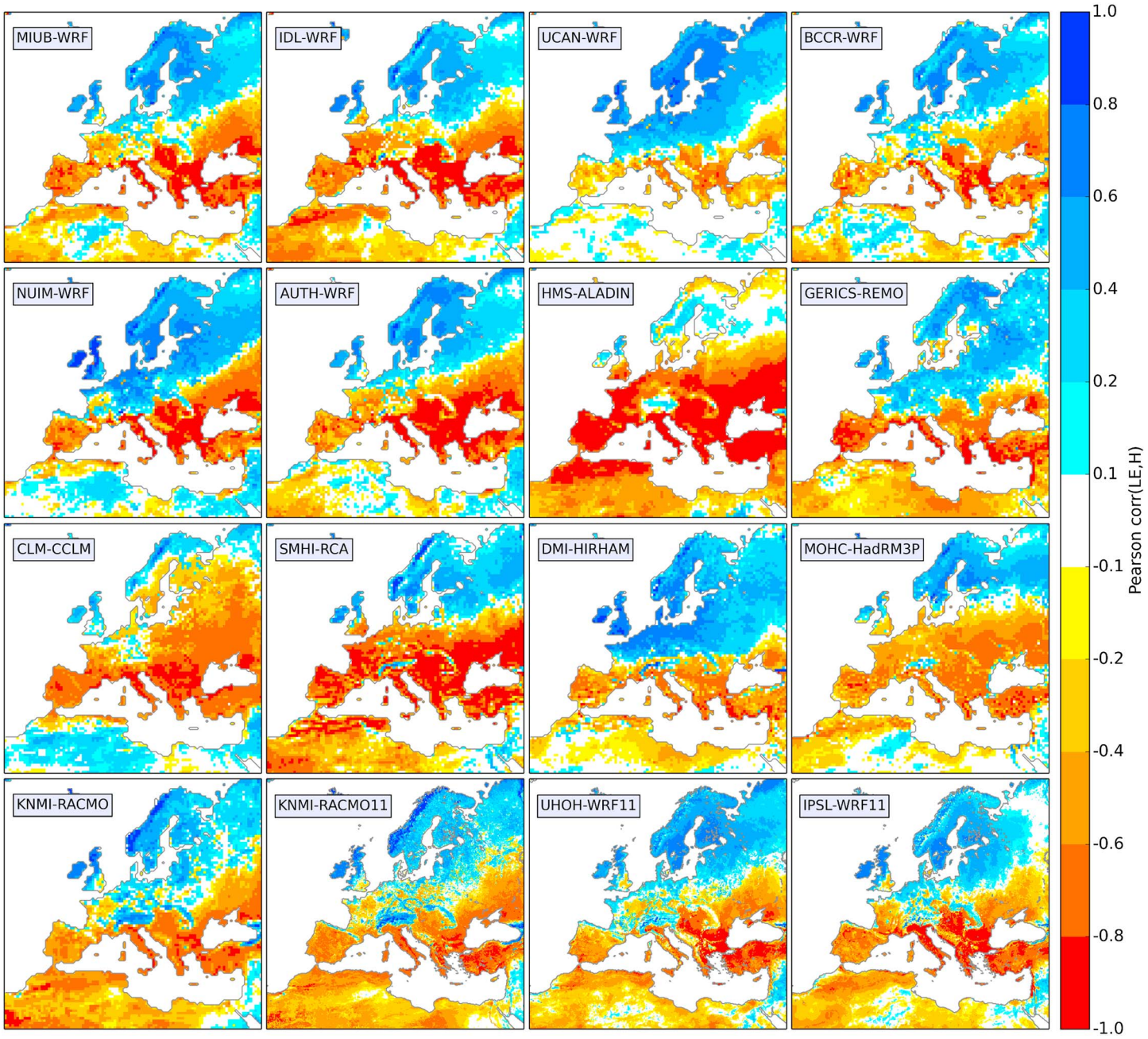

Figure 8. Correlation of summer (JJA) 10 day averages of latent and sensible heat flux for the years 1990 to 2008.

over grassland (NL-Ca1 and NL-Hor) than over forest (NL-Loo). To corroborate such relations, however, the number of stations in similar climatic regions is unfortunately too sparse.

4.2. EURO-CORDEX Ensemble Comparison to GLEAM

In addition to the correlation of latent and sensible heat flux, the following section investigates two process steps of the soil moisture-temperature coupling; first the connection of soil moisture to flux partitioning and second the connection of flux partitioning to atmospheric temperature which is defined as the second coupling metric that is applied in this study. The connection between soil moisture and flux partitioning is indicated by the correlation of the 10 day averaged summertime (JJA) evaporative fraction (ratio of latent heat to the sum of sensible and latent heat flux) and total (i.e., vertically integrated) soil

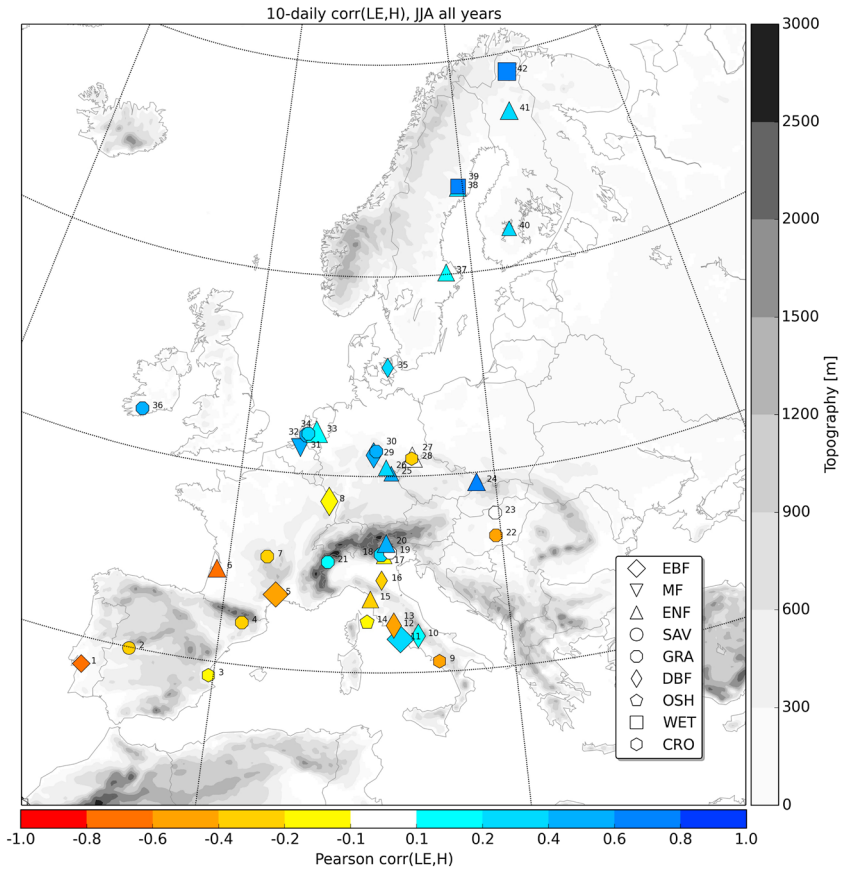

Figure 9. Correlations of 10 day mean observed summertime (JJA) latent and sensible heat flux for all available years at the FLUXNET stations. Only days for which all half-hourly values have a quality flag 0 or 1 (original data or high-quality gap filled) are taken into account, and only months with a minimum of 20 high-quality days. Symbols indicate the vegetation type (see Figure 1) at the station. The larger the size of the symbol the more high-quality data are available. Numbers refer to the individual stations as shown in Figure 10.

moisture (Figure 11). As decreasing (increasing) soil moisture leads to a decrease (increase) of the evaporative fraction, positive correlations are found over most of Europe in all model runs. Exceptions are the northern parts of Scandinavia and Russia and over the Alps, where the WRF runs, MOHC-HadRM3P and SMHI-RCA show no or even negative correlations. This behavior can most likely be attributed to a delayed thawing of frozen soil layers. When only the uppermost soil layer moisture is used (as possible for the WRF simulations), the correlation with the evaporative fraction is also positive. The noisy pattern in Northern Africa relates to the very dry conditions in summer with latent heat flux close to zero and soil moisture at its minimum. While all models show similar results for Europe, the DMI-HIRHAM model differently shows patterns of uncorrelated or even slightly negative correlations for the British Isles and parts of central and eastern Europe. Since both evaporative fraction and soil moisture are quite high in these regions, it is assumed to be an energy-limited regime where a small decrease in soil moisture does not much affect the flux partitioning.

The correlation of 10 daily averages of latent heat flux and 2 m air temperature is shown in Figure 12 for the 16 RCM simulations. The comparison of the individual RCMs gives a similar picture as the *H*-LE correlation in Figure 8 in the way that stronger than ensemble average coupling (e.g., HMS-ALADIN, CLM-CCLM, SMHI-RCA, and MOHC-HadRM3P) as well as weaker coupling (e.g., UCAN-WRF and DMI-HIRHAM) is identified for the same RCM simulations. Again, all simulations show a clear north-south-pattern with strong coupling in southern Europe and weak coupling in northern Europe. Overall, the LE-*T* correlation is slightly weaker than the *H*-LE correlation signal and the transition zone from positive to negative correlation is located further to the south. The first can be explained by the fact that LE-*T* correlation describes one step further in the land-atmosphere coupling process chain of changing soil moisture leading to changing fluxes leading to changing

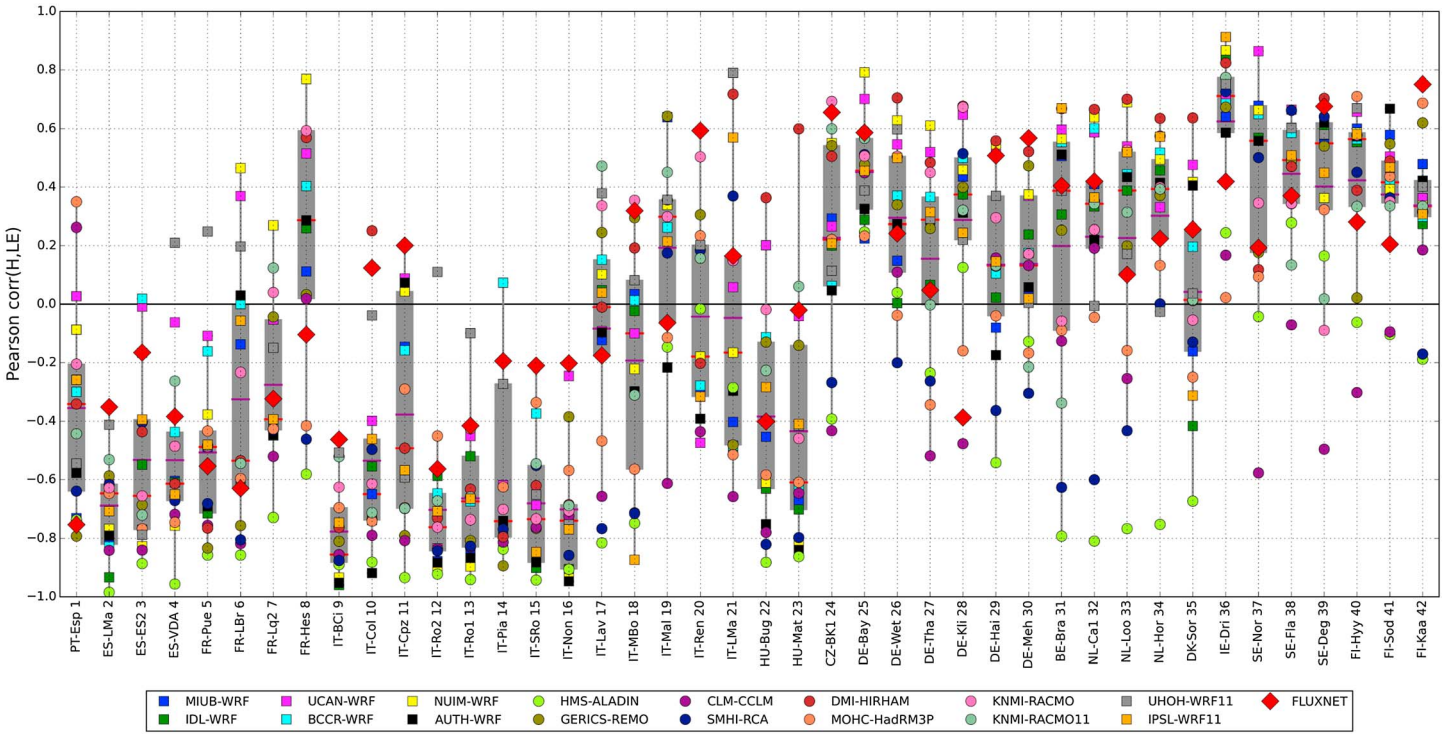

Figure 10. Correlations of 10-daily mean observed summertime (JJA) latent and sensible heat flux for all available years at the FLUXNET stations (big red diamonds); for station locations see Figure 1 (dots) and Figure 9 (the numbers on the *x* axis correspond to the station labeling in Figure 9). Small colored dots (and squares for WRF RCMs) indicate the *H*-LE correlation values of the individual RCMs at the nearest grid point to a FLUXNET station. The calculation is based on the same time spans for which observation data are available. Boxplots indicate the quantile range (gray), the medians (red line), and the means (purple line) of the RCM ensemble for each station. Stations are ordered geographically from south to north along the *x* axis.

temperature and that local temperature changes are also largely effected by advection. This fact also suggests that different coupling metrics cannot be directly compared in terms of absolute values even if it is a correlation-based metric ranging from −1 to 1.

With the GLEAM data set for evaporation and the ERA-Interim reanalysis for 2 m temperature a gridded observation-based reference for the LE-*T* correlation coupling metric is given in Figure 13. The averaged coupling strength of the 16 RCM ensemble is in overall good agreement with the observation-based pattern as both indicate strong coupling (negative correlations) for the Iberian Peninsula, Italy, southeastern Europe, and parts of France and weak coupling (positive correlations) for Scandinavia and northeastern Europe. The related difference plot shows that the ensemble mean coupling strength is stronger for large parts of central and eastern Europe and slightly weaker for the Iberian Peninsula and northern Scandinavia. Also, grid point wise counting the number of RCMs that simulate stronger coupling than GLEAM-ERAInt (red (blue) colors indicate more (less) than half of the ensemble) gives a similar picture.

The direct comparison of the individual RCMs and the GLEAM-ERAint LE-*T* correlation for the individual PRUDENCE regions is displayed in Figure 14. While a majority of RCMs agree with the GLEAM-ERAint correlation sign for all regions, the ensemble spread as expected from Figure 12 is quite large especially for France, middle Europe, the Alpine domain, and eastern Europe. For those regions, where coupling is either clearly weak (Scandinavia) or strong (Iberian Peninsula and Mediterranean) the RCMs differ less. In line with the maps in Figure 13 more than 75% of RCMs overestimate the observation-based coupling strength for middle Europe, the Alpine domain, the Mediterranean and eastern Europe. They predominantly show less strong coupling for the Iberian Peninsula, whereby all RCMs and the observation-based reference indicate negative LE-*T* correlation in this region. Compared to the individual station grid points in Figure 10 the RCM spread is less pronounced which mainly results from spatial averaging. The comparison to the GLEAM data product leads to more confidence in the FLUXNET based analysis (section 4.1): there is a tendency of the RCMs to overestimate coupling strength, albeit this does not yield for all regions. Please note that this is also based

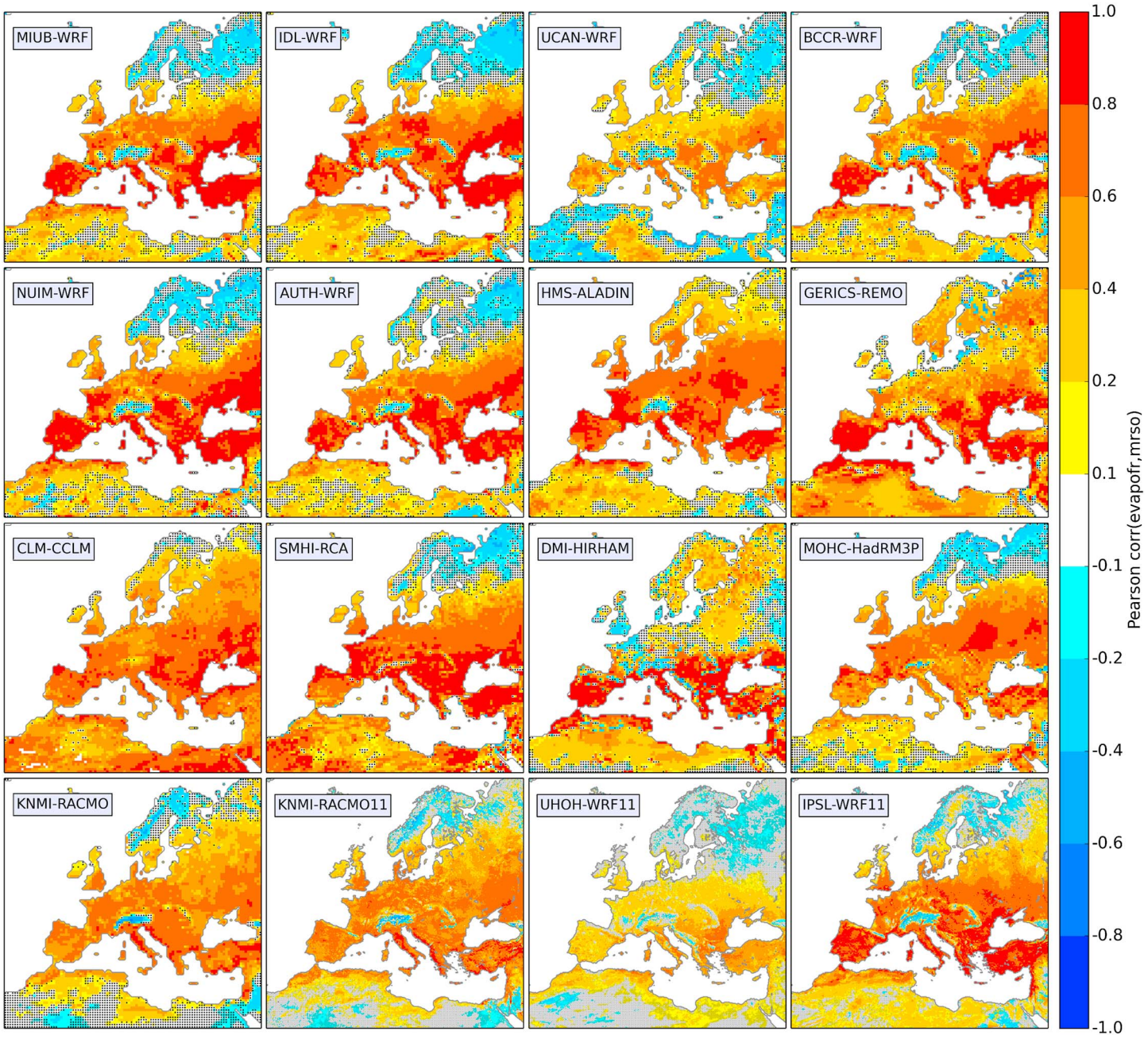

Figure 11. Correlation between 10 day averages of total soil moisture and the evaporative fraction computed for the summers between 1990 and 2008 (dotted where correlation is below 5% significance level).

on the assumption that the GLEAM-ERAint is the perfect benchmark. Though both GLEAM and ERA-Interim are well established and thoroughly evaluated data sets, they are also based on models that may have the same constraints in the ability of simulating the soil and land surface processes correctly. Still we consider it as a most fair reference for the purpose of this study.

5. Summary and Conclusions

This study investigates the land-atmosphere coupling in a EURO-CORDEX reanalysis-driven ensemble in a two-step approach. First, the simulated soil moisture and turbulent surface energy fluxes are compared to satellite-based soil moisture estimates from the GLEAM data set and measurements from a set of

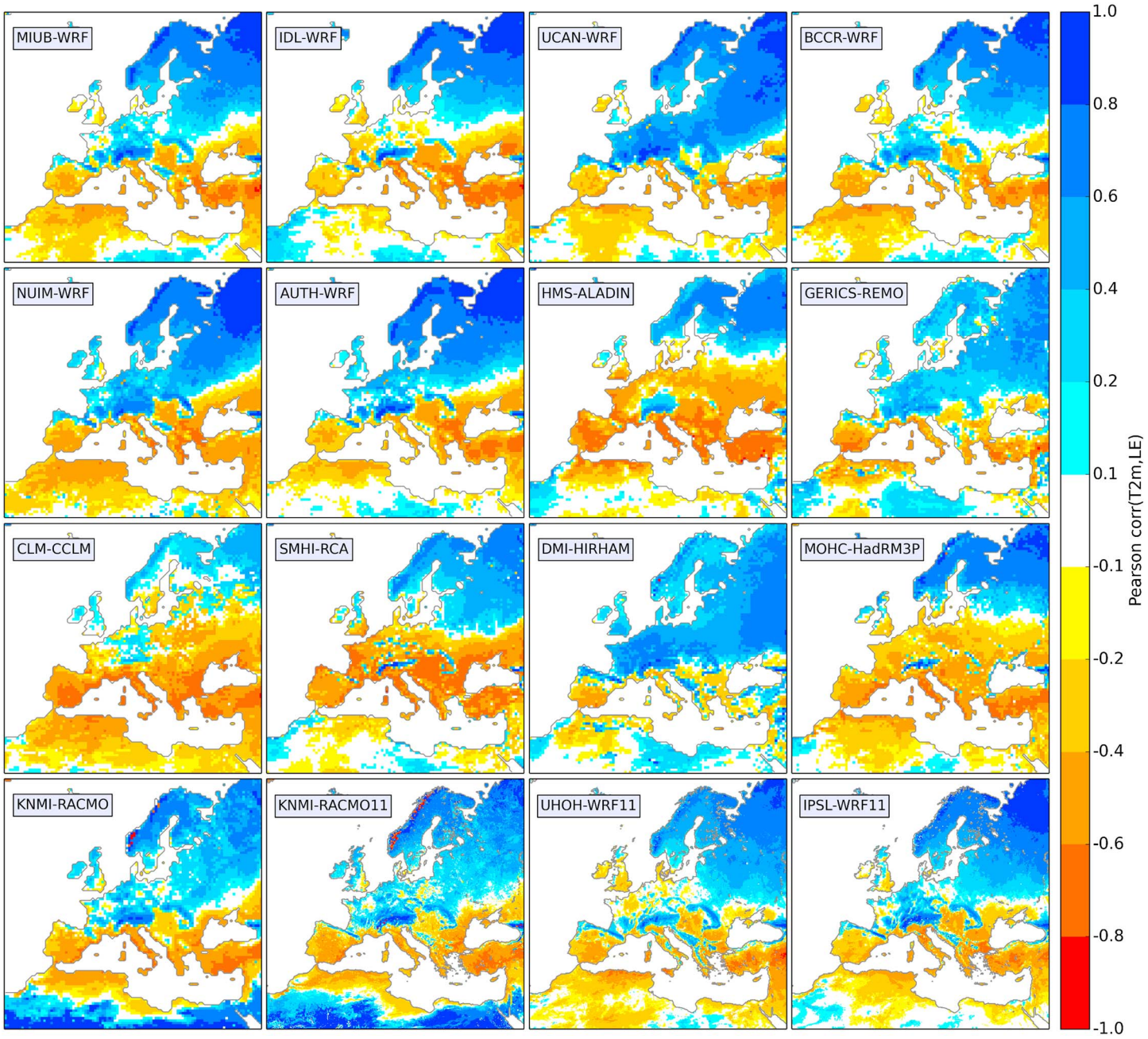

Figure 12. Correlation of summer (JJA) 10 day averages of latent heat flux and air temperature (2 m) for the years 1990 to 2008.

European FLUXNET sites. Then, based on two coupling strength metrics, coupling regimes and transition zones are identified, differences in the RCM ensemble are assessed, and simulated coupling strength is compared with results from FLUXNET and GLEAM.

The individual models generally agree on the large-scale patterns corresponding to the European climate zones, but regionally, the spread of results can be large. The RCMs' total soil moisture time series averaged over the PRUDENCE regions show clear annual cycles with largest amplitudes in southern Europe and also reasonable interannual variability according to the weather conditions in the individual years. For the majority of the RCMs the soil moisture is positively correlated with GLEAM soil moisture for large parts of Europe, strongest for the Iberian Peninsula and the British Isles, but less correlated for parts of eastern Europe.

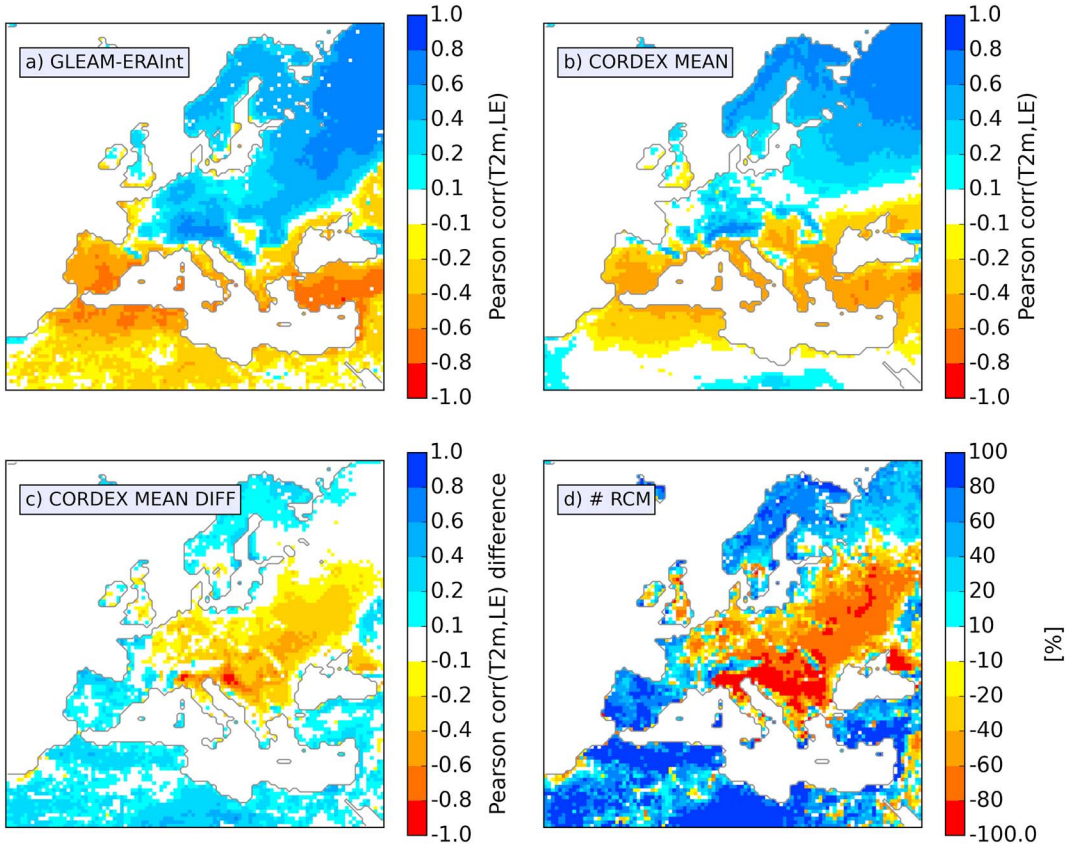

Figure 13. (a) Correlation of latent heat flux and air temperature (2 m) for GLEAM (LE) and ERA-Interim (*T*), (b) for the ensemble mean of Figure 13, and (c) for the difference of Figures 13b minus 13a. (d) Percentage of RCMs that simulate stronger (red) or weaker (blue) coupling strength than GLEAM-ERAInt.

The expected flux partitioning following the European climate regions is fairly well reproduced by the RCM ensemble and also in accordance with representative FLUXNET observations. The partially large ensemble spread can most probably be attributed on the one hand side to differing LSM parametrizations including assumptions concerning vegetation and soil-type distributions. A benchmarking intercomparison by *Best et al*. [2015] revealed that LSMs still have deficits in the correct representation of the fluxes and do not appropriately use the information available in the atmospheric forcing data. While it is not feasible for the ensemble of opportunity to define a benchmark in the sense of an a priori expectation on the results, we support the suggestion by *Best et al*. [2015] that developing benchmark metrics that can assess the whole coupled system would be an ultimate objective.

For the EURO-CORDEX RCM simulations the diversity in the simulated fluxes partly results from different sets of atmospheric parametrizations, which impact the simulated regional weather conditions. This influence can be inferred from a subset of WRF simulations which use the same LSM: some members produce regionally higher overall surface energy fluxes due to higher solar radiation caused by less cloudiness in response to different convection and microphysics parameterizations. Multiple feedbacks between land surface and atmospheric processes result in differences in, e.g., mean 2 m air temperature and total precipitation (as analyzed in other evaluation studies [*Kotlarski et al*., 2014; *Katragkou et al*., 2015]). These differences, however, depend on many model parameters and cannot be directly or exclusively linked with coupling properties of the individual RCMs.

The land-atmosphere coupling strength is investigated both in observations and simulations via two integrative metrics based on the correlation between sensible and latent heat fluxes and the correlation of latent heat flux and 2 m air temperature, respectively, which describe the strength of soil moisture-related feedback processes. A major advantage of these methods is its easy applicability to both standard RCM output, on

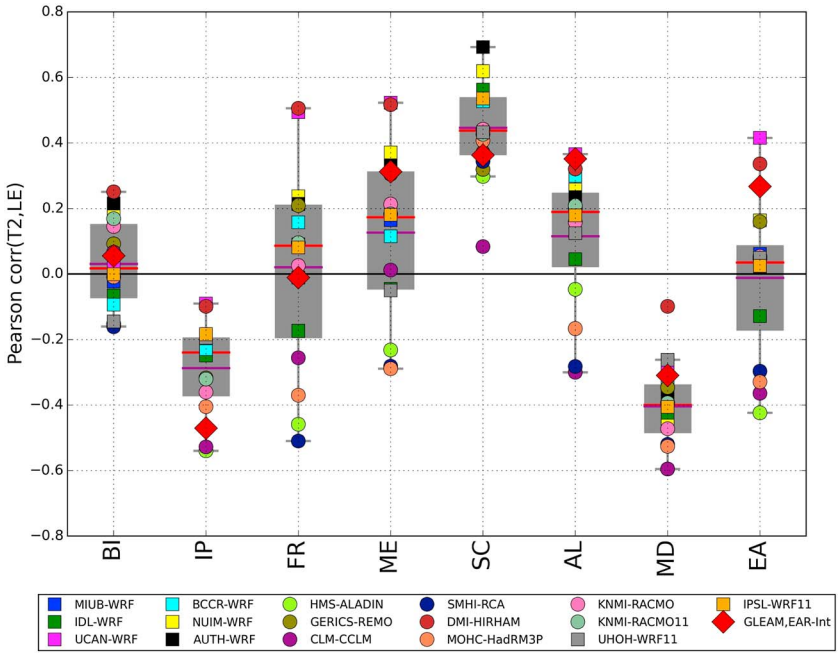

Figure 14. Correlations of 10-daily mean summertime (JJA) latent heat flux and air temperature for the years 1990–2008 averaged for different PRUDENCE regions. Boxplots indicate the quantile range (gray), the medians (red line), and the means (purple line) of the RCM ensemble for each region. The big red diamonds show the LE-*T* correlation of GLEAM-ERAInt.

which we had to rely in this study, based on an ensemble of opportunity, and to the FLUXNET observations (for *H*-LE correlation) as well as to the gridded GLEAM-ERAInt observation-based data (LE-*T* correlation).

The coupling strength analysis of the EURO-CORDEX simulations based on *H*-LE correlation for the summer months (JJA) over the period 1990 to 2008 revealed strong coupling in southern Europe and weak coupling in northern Europe for all members of a multimodel ensemble in overall agreement with the FLUXNET measurements. In the transition zone over large parts of central Europe between these coupling regimes the RCMs diverge and show a wide range of coupling strengths. There is a tendency toward a stronger coupling in the RCMs with reference to the FLUXNET observations, but the relatively small number of sufficiently long and high-quality observation time series for many regions limits the confidence of that conclusion.

The comparison of the LE-*T* correlation derived from the RCM results and from the gridded GLEAM-ERAInt reference, however, corroborates the statement that the majority of RCMs overestimates the coupling strength for large parts of Europe. This is consistent with evaluation studies on global models that reveal an overestimation of land-atmosphere coupling in the midlatitudes [*Sippel et al*., 2016] and parts of the U.S. [*Merrifield and Xie*, 2016].

Both metrics agree in attributing stronger and weaker coupling strength than average to individual RCMs. While both show the typical north-south pattern for Europe, the transition from positive to negative correlation is slightly shifted to the south for the LE-*T* correlation metric. Overall the detected regions for strong coupling in southern Europe agree with previous studies based on global models [*Koster et al*., 2006; *Dirmeyer*, 2011], regional models [*Seneviratne et al*., 2006; *Jaeger et al*., 2009], and observations [*Miralles et al*., 2012] for a similar time span but using different experiment designs and coupling metrics. Our results also support the suggestion by *Lorenz et al*. [2015] that the coupling strength derived from different metrics may provide similar information although they cannot be directly compared in their absolute values unless appropriately scaled. Consistent, but inevitably computationally expensive GLACE-type experiments like those by *Koster et al*. [2006], *Seneviratne et al*. [2006], or *Hirsch et al*. [2014] for all RCMs would allow for a more robust assessment of coupling strength than possibly with the ensemble of opportunity at hand. Nevertheless, the relatively simple correlation-based coupling metrics are suitable for an intercomparison of different RCM runs. The coupling metrics provide additional information for the explanation of differences

we see in, e.g., extreme temperatures that show positive biases for the more strongly coupled RCMs. Finer model resolutions generate additional small-scale heterogeneities in coupling strength, but these seem not to affect the large-scale coupling patterns. In order to corroborate this statement, however, a larger number of direct comparisons of EUR-11 and EUR-44 simulations with the same RCM are required.

The strength of land-atmosphere coupling varies across seasons and regions, and it is expected to become stronger in the context of a warming climate, especially in locations where this feedback plays an important role [*Seneviratne et al*., 2006; *Dirmeyer et al*., 2014]. Therefore, the models' ability to properly simulate coupling strength is highly relevant as it, e.g., influences the representation of heat waves. A follow-up study will analyze the mechanisms and speed of a possible intensification of the coupling strength and the northward shift of the transition zone using the EURO-CORDEX ensemble of control simulations and future regional climate change scenarios.

Acknowledgments
The authors like to thank the coordination and the participating institutes of the EURO-CORDEX initiative for making this study possible. The contribution from Centre de Recherche Public-Gabriel Lippmann (labeled here as "MIUB") (now Luxembourg Institute of Science and Technology, LIST) was funded by the Luxembourg National Research Fund (FNR) through grant FNR C09/SR/16 (CLIMPACT). The John von Neumann Institute for Computing and the Forschungszentrum Jülich provided the required compute time for the project JJSC15. Work is furthermore sponsored through a research and development cooperation on hydrometeorology between the Federal Institute of Hydrology, Koblenz, Germany, and the Meteorological Institute, University of Bonn, Bonn, Germany. The KNMI-RACMO simulation was supported by the Dutch Ministry of Infrastructure and the Environment. The simulations of the Universidad de Cantabria were supported by the CORWES project (CGL2010-22158-C02), funded by the Spanish R&D Programme and by the FP7 grant 308291 (EUPORIAS). We acknowledge Santander Supercomputacion support group at the University of Cantabria, who provided access to the Altamira Supercomputer at the Institute of Physics of Cantabria (IFCA-CSIC), member of the Spanish Supercomputing Network. Rowan Fealy acknowledges the financial support provided by the Irish Environmental Protection Agency and the use of Maynooth University's high-performance computer and the Irish Centre for High End Computing (ICHEC) Stokes facility. The work done by Rita M. Cardoso and Pedro M.M. Soares was financed the Portuguese Science Foundation (FCT) under Project SOLAR-PTDC/GEOMET/7078/2014. The work of University of Hohenheim as part of the Project RU 1695 was funded by German Science Foundation (DFG). WRF-UHOH simulations were carried out at the supercomputing center HLRS in Stuttgart (Germany). The CLMcom-CCLM simulation was supported by the German Federal Ministry of Education and Research (BMBF) and the German Climate Computing Centre (DKRZ). AUTH-DMC acknowledges the technical support of AUTH-Scientific Computing Center, the HellasGrid/EGI infrastructure, and the financial support of AUTH-Research Committee (Pr.Nr. 91376 and 87783). This work used eddy covariance data acquired by the FLUXNET community. We acknowledge the financial support to the eddy covariance data harmonization (www.fluxdata.org). The

References

Armstrong, R. L., M. J. Brodzik, K. Knowles, and M. Savoie (2005), Global monthly EASE-Grid snow water equivalent climatology, *Digit. Media*, doi:10.5067/KJVERY3MIBPS.

Bachner, S., A. Kapala, and C. Simmer (2008), Evaluation of daily precipitation characteristics in the CLM and their sensitivity to parameterizations, *Meteorol. Z.*, *17*(4), 407–419, doi:10.1127/0941-2948/2008/0300.

Baldauf, M., and J. P. Schulz (2004), Prognostic precipitation in the Lokal-Modell (LM) of DWD, *Cosmo Newsl.*, *4*, 177–180.

Baldocchi, D., et al. (2001), FLUXNET: A new tool to study the temporal and spatial variability of ecosystem-scale carbon dioxide, water vapor, and energy flux densities, *Bull. Am. Meteorol. Soc.*, *82*(11), 2415–2434, doi:10.1175/1520-0477(2001)082<2415:FANTTS>2.3.CO;2.

Balsamo, G., A. Beljaars, K. Scipal, P. Viterbo, B. van den Hurk, M. Hirschi, and A. K. Betts (2009), A revised hydrology for the ECMWF model: Verification from field site to terrestrial water storage and impact in the integrated forecast system, *J. Hydrometeorol.*, *10*(3), 623–643, doi:10.1175/2008JHM1068.1.

Beck, H. E., A. I. J. M. van Dijk, V. Levizzani, J. Schellekens, D. G. Miralles, B. Martens, and A. de Roo (2016), MSWEP: 3-hourly 0.25° global gridded precipitation (1979–2015) by merging gauge, satellite, and reanalysis data, *Hydrol. Earth Syst. Sci. Discuss.*, 1–38, doi:10.5194/hess-2016-236.

Best, M. J., et al. (2015), The plumbing of land surface models: Benchmarking model performance, *J. Hydrometeorol.*, *16*, 1425–1442, doi:10.1175/JHM-D-14-0158.1.

Betts, A. K., R. Desjardins, A. C. M. Beljaars, and A. Tawfik (2015), Observational study of land-surface-cloud-atmosphere coupling on daily timescales, *Front. Earth Sci.*, *3*, doi:10.3389/feart.2015.00013.

Bougeault, P. (1985), A simple parameterization of the large scale effect of cumulus convection, *Mon. Weather Rev.*, *113*, 2108–2121, doi:10.1175/1520-0493(1985)113<2108:ASPOTL>2.0.CO;2.

Casanueva, A., et al. (2015), Daily precipitation statistics in a EURO-CORDEX RCM ensemble: Added value of raw and bias-corrected high-resolution simulations, *Clim. Dyn.*, 1–19, doi:10.1007/s00382-015-2865-x.

Champeaux, J. L., V. Masson, and F. Chauvin (2005), ECOCLIMAP: A global database of land surface parameters at 1 km resolution, *Meteorol. Appl.*, *12*(1), 29–32, doi:10.1017/S1350482705001519.

Christensen, J. H., and O. B. Christensen (2007), A summary of the PRUDENCE model projections of changes in European climate by the end of this century, *Clim. Change*, *81*(S1), 7–30, doi:10.1007/s10584-006-9210-7.

Claussen, M., U. Lohmann, E. Roeckner, and U. Schulzweida (1994), A global data set of land-surface parameters.

Collins, W. D., P. J. Rasch, B. A. Boville, J. J. Hack, J. R. McCaa, D. L. Williamson, J. T. Kiehl, and B. Briegleb (2004), Description of the NCAR community atmosphere model (CAM 3.0), *NCAR Tech. Note NCAR/TN-464+ STR*, (June).

Cuxart, J., P. Bougeault, and J.-L. Redelsperger (2000), A turbulence scheme allowing for mesoscale and large-eddy simulations, *Q. J. R. Meteorol. Soc.*, *126*(562), 1–30, doi:10.1002/qj.49712656202.

Decker, M., A. Pitman, and J. Evans (2015), Diagnosing the seasonal land–atmosphere correspondence over northern Australia: Dependence on soil moisture state and correspondence strength definition, *Hydrol. Earth Syst. Sci.*, *1*, 3433–3447, doi:10.5194/hess-19-3433-2015.

Dee, D. P., et al. (2011), The ERA-Interim reanalysis: Configuration and performance of the data assimilation system, *Q. J. R. Meteorol. Soc.*, *137*(656), 553–597, doi:10.1002/qj.828.

Dirmeyer, P. a. (2011), The terrestrial segment of soil moisture-climate coupling, *Geophys. Res. Lett.*, *38*, L16702, doi:10.1029/2011GL048268.

Dirmeyer, P. A., Z. Wang, M. J. Mbuh, and H. E. Norton (2014), Intensified land surface control on boundary layer growth in a changing climate, *Geophys. Res. Lett.*, *41*, 1290–1294, doi:10.1002/2013GL058826.

Doms, G., et al. (2011), Consortium for small-scale modelling: A description of the nonhydrostatic regional COSMO model. Part II: Physical parameterization.

Edwards, J. M., and A. Slingo (1995), Studies with a flexible new radiation code. I: Choosing a configuration for a large-scale model, *Q. J. R. Meteorol. Soc.*, *122*, 689–719, doi:10.1002/qj.49712253107.

Ek, M. B., K. E. Mitchell, Y. Lin, E. Rogers, P. Grunmann, V. Koren, G. Gayno, and J. D. Tarpley (2003), Implementation of Noah land surface model advances in the National Centers for Environmental Prediction operational mesoscale Eta model, *J. Geophys. Res.*, *108*(D22), 8851, doi:10.1029/2002JD003296.

Essery, R. L. H., M. J. Best, R. A. Betts, P. M. Cox, and C. M. Taylor (2003), Explicit representation of subgrid heterogeneity in a GCM land surface scheme, *J. Hydrometeorol.*, *4*(3), 530–543, doi:10.1175/1525-7541(2003)004<0530:EROSHI>2.0.CO;2.

Findell, K. L., P. Gentine, B. R. Lintner, and C. Kerr (2011), Probability of afternoon precipitation in eastern United States and Mexico enhanced by high evaporation, *Nat. Geosci.*, *4*(7), 434–439, doi:10.1038/ngeo1174.

Fischer, E. M., S. I. Seneviratne, P. L. Vidale, D. Lüthi, and C. Schär (2007), Soil moisture–atmosphere interactions during the 2003 European summer heat wave, *J. Clim.*, *20*(20), 5081–5099, doi:10.1175/JCLI4288.1.

Flato, G., et al. (2013), Evaluation of climate models, in *Climate Change 2013 Physics Science Basis. Contribution of Working Group I to the Fifth Assessment Report of the Intergovernmental Panel on Climate Change*, edited by T. F. Stocker, pp. 741–866, Cambridge Univ. Press, Cambridge, U. K., and New York, doi:10.1017/CBO9781107415324.

ERA-Interim data were accessed from http://apps.ecmwf.int/datasets/. The GLEAM data were accessed from www.gleam.eu/#downloads. The analysis results and the underlying RCM data base are available upon request (sknist@uni-bonn.de). The data are archived at the Jülich Supercomputing Centre, Research Centre Jülich, Jülich, Germany. We thank the anonymous reviewers for their detailed and constructive comments.

Fouquart, Y., and B. Bonnel (1980), Computations of solar heating of the earth's atmosphere—A new parameterization, *Beiträge Phys. Atmos.*, *53*, 35–62.

Froidevaux, P., L. Schlemmer, J. Schmidli, W. Langhans, and C. Schär (2014), Influence of the background wind on the local soil moisture–precipitation feedback, *J. Atmos. Sci.*, *71*(2), 782–799, doi:10.1175/JAS-D-13-0180.1.

García-Díez, M. (2014), Physical realism, added value and sensitivity to parameterizations of a Regional Climate Model over Europe, Universidad de Cantabria.

García-Díez, M., J. Fernández, and R. Vautard (2015), An RCM multi-physics ensemble over Europe: Multi-variable evaluation to avoid error compensation, *Clim. Dyn.*, doi:10.1007/s00382-015-2529-x.

Giorgi, F., C. Jones, and G. R. Asrar (2009), Addressing climate information needs at the regional level: The CORDEX framework, *WMO Bull.*, *58*, 175–183.

Gregory, D., and P. R. Rowntree (1990), A mass flux convection scheme with representation of cloud ensemble characteristics and stability-dependent closure, *Mon. Weather Rev.*, *118*(7), 1483–1506, doi:10.1175/1520-0493(1990)118<1483:AMFCSW>2.0.CO;2.

Gregory, D., R. Kershaw, and P. M. Inness (1997), Parametrization of momentum transport by convection. II: Tests in single-column and general circulation models, *Q. J. R. Meteorol. Soc.*, *123*(541), 1153–1183, doi:10.1002/qj.49712354103.

Grell, G. A., and D. Dévényi (2002), A generalized approach to parameterizing convection combining ensemble and data assimilation techniques, *Geophys. Res. Lett.*, *29*(14), 1693, doi:10.1029/2002GL015311.

Greve, P., K. Warrach-Sagi, and V. Wulfmeyer (2013), Evaluating soil water content in a WRF-Noah downscaling experiment, *J. Appl. Meteorol. Climatol.*, *52*(10), 2312–2327, doi:10.1175/JAMC-D-12-0239.1.

Guillod, B. P., et al. (2013), Land surface controls on afternoon precipitation diagnosed from observational data: Uncertainties, confounding factors and the possible role of vegetation interception, *Atmos. Chem. Phys. Discuss.*, *13*(11), 29,137–29,201, doi:10.5194/acpd-13-29137-2013.

Hagemann, S. (2002), An improved land surface parameter dataset for global and regional climate models, *MPI Rep.*, *336*(336), 1–21.

Hansen, M. C., R. S. Defries, J. R. G. Townshend, and R. Sohlberg (2000), Global land cover classification at 1 km spatial resolution using a classification tree approach, *Int. J. Remote Sens.*, *21*(6–7), 1331–1364.

Hirsch, A. L., A. J. Pitman, S. I. Seneviratne, J. P. Evans, and V. Haverd (2014), Summertime maximum and minimum temperature coupling asymmetry over Australia determined using WRF, *Geophys. Res. Lett.*, *41*, 1546–1552, doi:10.1002/2013GL059055.

Hirschi, M., B. Mueller, W. Dorigo, and S. I. Seneviratne (2014), Using remotely sensed soil moisture for land–atmosphere coupling diagnostics: The role of surface vs. root-zone soil moisture variability, *Remote Sens. Environ.*, *154*, 246–252, doi:10.1016/j.rse.2014.08.030.

Hohenegger, C., P. Brockhaus, C. S. Bretherton, and C. Schär (2009), The soil moisture–precipitation feedback in simulations with explicit and parameterized convection, *J. Clim.*, *22*(19), 5003–5020, doi:10.1175/2009JCLI2604.1.

Hong, S., and J. Lim (2006), The WRF single-moment 6-class microphysics scheme (WSM6), *J. Korean Meteorol. Soc.*, *42*(2), 129–151.

Hong, S.-Y., J. Dudhia, and S.-H. Chen (2004), A revised approach to ice microphysical processes for the bulk parameterization of clouds and precipitation, *Mon. Weather Rev.*, *132*(1), 103–120, doi:10.1175/1520-0493(2004)132<0103:ARATIM>2.0.CO;2.

Hong, S.-Y., Y. Noh, and J. Dudhia (2006), A new vertical diffusion package with an explicit treatment of entrainment processes, *Mon. Weather Rev.*, 2318–2341.

Iacono, M. J., J. S. Delamere, E. J. Mlawer, M. W. Shephard, S. A. Clough, and W. D. Collins (2008), Radiative forcing by long-lived greenhouse gases: Calculations with the AER radiative transfer models, *J. Geophys. Res.*, *113*, D13103, doi:10.1029/2008JD009944.

Ingwersen, J., et al. (2011), Comparison of Noah simulations with eddy covariance and soil water measurements at a winter wheat stand, *Agric. For. Meteorol.*, *151*(3), 345–355, doi:10.1016/j.agrformet.2010.11.010.

Jaeger, E. B., R. Stöckli, and S. I. Seneviratne (2009), Analysis of planetary boundary layer fluxes and land-atmosphere coupling in the regional climate model CLM, *J. Geophys. Res.*, *114*, D17106, doi:10.1029/2008JD011658.

Janjić, Z. I. (1994), The step-mountain eta coordinate model: Further developments of the convection, viscous sublayer, and turbulence closure schemes, *Mon. Weather Rev.*, *122*(5), 927–945, doi:10.1175/1520-0493(1994)122<0927:TSMECM>2.0.CO;2.

Joint Research Centre: Global land cover 2000 database (2003), European Commission, Joint Research Centre. [Available at http://bioval.jrc.ec.europa.eu/products/glc2000/glc2000.php, accessed 2016-12-21.]

Kain, J. S. (2004), The Kain–Fritsch convective parameterization: An update, *J. Appl. Meteorol.*, *43*(1), 170–181, doi:10.1175/1520-0450(2004)043<0170:TKCPAU>2.0.CO;2.

Kain, J. S., and J. M. Fritsch (1993), *The Representation of Cumulus Convection in Numerical Models*, edited by K. A. Emanuel and D. J. Raymond, pp. 165–170, Am. Meteorol. Soc., Boston, Mass.

Katragkou, E., et al. (2015), Regional climate hindcast simulations within EURO-CORDEX: Evaluation of a WRF multi-physics ensemble, *Geosci. Model Dev.*, *8*(3), 603–618, doi:10.5194/gmd-8-603-2015.

Koster, R. D., et al. (2006), GLACE: The Global Land–Atmosphere Coupling Experiment. Part I: Overview, *J. Hydrometeorol.*, *7*(4), 590–610, doi:10.1175/JHM510.1.

Kotlarski, S., et al. (2014), Regional climate modeling on European scales: A joint standard evaluation of the EURO-CORDEX RCM ensemble, *Geosci. Model Dev. Discuss.*, *7*(1), 217–293, doi:10.5194/gmdd-7-217-2014.

Lenderink, G., and A. A. M. Holtslag (2004), An updated length-scale formulation for turbulent mixing in clear and cloudy boundary layers, *Q. J. R. Meteorol. Soc.*, *130*(604), 3405–3427, doi:10.1256/qj.03.117.

Liu, Y. Y., R. M. Parinussa, W. A. Dorigo, R. A. M. De Jeu, W. Wagner, A. I. J. M. van Dijk, M. F. McCabe, and J. P. Evans (2011a), Developing an improved soil moisture dataset by blending passive and active microwave satellite-based retrievals, *Hydrol. Earth Syst. Sci.*, *15*(2), 425–436, doi:10.5194/hess-15-425-2011.

Liu, Y. Y., R. A. M. De Jeu, M. F. McCabe, J. P. Evans, and A. I. J. M. Van Dijk (2011b), Global long-term passive microwave satellite-based retrievals of vegetation optical depth, *Geophys. Res. Lett.*, *38*, L18402, doi:10.1029/2011GL048684.

Lohmann, U., and E. Roeckner (1996), Design and performance of a new cloud microphysics scheme developed for the ECHAM general circulation model, *Clim. Dyn.*, *12*(8), 557–572, doi:10.1007/BF00207939.

Lorenz, R., A. J. Pitman, A. L. Hirsch, and J. Srbinovsky (2015), Intraseasonal versus interannual measures of land-atmosphere coupling strength in a global climate model: GLACE-1 versus GLACE-CMIP5 experiments in ACCESS1.3b, *J. Hydrometeorol.*, *16*(5), 2276–2295, doi:10.1175/JHM-D-14-0206.1.

Louis, J. F. (1979), A parametric model of vertical eddy fluxes in the atmosphere, *Boundary Layer Meteorol.*, *17*(2), 187–202, doi:10.1007/BF00117978.

Martens, B., D. G. Miralles, H. Lievens, R. van der Schalie, R. A. M. de Jeu, D. Férnandez-Prieto, H. E. Beck, W. A. Dorigo, and N. E. C. Verhoest (2016), GLEAM v3: Satellite-based land evaporation and root-zone soil moisture, *Geosci. Model Dev. Discuss.*, 1–36, doi:10.5194/gmd-2016-162.

Martin, G. M., D. W. Johnson, and A. Spice (1994), The measurement and parameterization of effective radius of droplets in warm stratocumulus clouds, *J. Atmos. Sci.*, *51*(13), 1823–1842, doi:10.1175/1520-0469(1994)051<1823:TMAPOE>2.0.CO;2.

Massey, N., R. Jones, F. E. L. Otto, T. Aina, S. Wilson, J. M. Murphy, D. Hassell, Y. H. Yamazaki, and M. R. Allen (2015), Weather@Home—Development and validation of a very large ensemble modelling system for probabilistic event attribution, *Q. J. R. Meteorol. Soc.*, *141*(690), 1528–1545, doi:10.1002/qj.2455.

Masson, V., J.-L. Champeaux, F. Chauvin, C. Meriguet, and R. Lacaze (2003), A global database of land surface parameters at 1 km resolution in meteorological and climate models, *J. Clim.*, *16*(9), 1261–1282.

Masson, V., et al. (2013), The SURFEXv7.2 land and ocean surface platform for coupled or offline simulation of Earth surface variables and fluxes, *Geosci. Model Dev.*, *6*(4), 929–960, doi:10.5194/gmd-6-929-2013.

Mengelkamp, H. T., et al. (2006), Evaporation over a heterogeneous land surface: The EVA-GRIPS project, *Bull. Am. Meteorol. Soc.*, *87*(6), 775–786, doi:10.1175/BAMS-87-6-775.

Merrifield, A. L., and S. P. Xie (2016), Summer U.S. surface air temperature variability: Controlling factors and AMIP simulation biases, *J. Clim.*, *29*(14), 5123–5139, doi:10.1175/JCLI-D-15-0705.1.

Milovac, J., K. Warrach-Sagi, A. Behrendt, F. Späth, J. Ingwersen, and V. Wulfmeyer (2016), Investigation of PBL schemes combining the WRF model simulations with scanning water vapor differential absorption lidar measurements, *J. Geophys. Res. Atmos.*, *121*, 624–649, doi:10.1002/2015JD023927.

Miralles, D. G., M. J. van den Berg, A. J. Teuling, and R. A. M. de Jeu (2012), Soil moisture-temperature coupling: A multiscale observational analysis, *Geophys. Res. Lett.*, *39*, L21707, doi:10.1029/2012GL053703.

Mlawer, E. J., S. J. Taubman, P. D. Brown, M. J. Iacono, and S. A. Clough (1997), Radiative transfer for inhomogeneous atmospheres: RRTM, a validated correlated-k model for the longwave, *J. Geophys. Res.*, *102*(D14), 16,663–16,682, doi:10.1029/97JD00237.

Morcrette, J.-J., L. Smith, and Y. Fouquart (1986), Pressure and temperature dependence of the absorption in longwave radiation parametrizations, *Beiträge Phys. Atmos.*, *59*(4), 455–469.

Morrison, H., G. Thompson, and V. Tatarskii (2009), Impact of cloud microphysics on the development of trailing stratiform precipitation in a simulated squall line: Comparison of one- and two-moment schemes, *Mon. Weather Rev.*, *137*(3), 991–1007, doi:10.1175/2008MWR2556.1.

Neggers, R. A. J. (2009), A dual mass flux framework for boundary layer convection. Part II: Clouds, *J. Atmos. Sci.*, *66*(6), 1489–1506, doi:10.1175/2008JAS2636.1.

Neggers, R. A. J., M. Köhler, and A. C. M. Beljaars (2009), A dual mass flux framework for boundary layer convection. Part I: Transport, *J. Atmos. Sci.*, *66*(6), 1465–1487, doi:10.1175/2008JAS2635.1.

Nordeng, T. E. (1994), Extended versions of the convection parametrization scheme at ECMWF and their impact upon the mean climate and transient activity of the model in the tropics, *Reading. Tech. rep. Res. Dept Tech. Memo*.

Prein, A. F., et al. (2015), Precipitation in the EURO-CORDEX 0.11° and 0.44° simulations: High resolution, High benefits?, *Clim. Dyn.*, doi:10.1007/s00382-015-2589-y.

Rahman, M., M. Sulis, and S. J. Kollet (2015), The subsurface–land surface–atmosphere connection under convective conditions, *Adv. Water Resour.*, *83*, 240–249, doi:10.1016/j.advwatres.2015.06.003.

Rasch, P. J., and J. E. Kristjánsson (1998), A comparison of the CCM3 model climate using diagnosed and predicted condensate parameterizations, *J. Clim.*, *11*(7), 1587–1614, doi:10.1175/1520-0442(1998)011<1587:ACOTCM>2.0.CO;2.

Rechid, D., S. Hagemann, and D. Jacob (2009), Sensitivity of climate models to seasonal variability of snow-free land surface albedo, *Theor. Appl. Climatol.*, *95*(1–2), 197–221, doi:10.1007/s00704-007-0371-8.

Ricard, J. L., and J. F. Royer (1993), A statistical cloud scheme for use in an AGCM, *Ann. Geophys.*, *11*, 1095–1115.

Ritter, B., and J.-F. Geleyn (1992), A comprehensive radiation scheme for numerical weather prediction models with potential applications in climate simulations, *Mon. Weather Rev.*, *120*(2), 303–325, doi:10.1175/1520-0493(1992)120<0303:ACRSFN>2.0.CO;2.

Samuelsson, P., S. Gollvik, and A. Ullerstig (2006), *The Land-Surface Scheme of the Rossby Centre Regional Atmospheric Climate Model (RCA3)*, *SMHI Meteorol.*, pp. 25, SMHI, SE-601 76 Norrköping, Sweden.

Santanello, J. a., C. D. Peters-Lidard, S. V. Kumar, C. Alonge, and W.-K. Tao (2009), A modeling and observational framework for diagnosing local land–atmosphere coupling on diurnal time scales, *J. Hydrometeorol.*, *10*(3), 577–599, doi:10.1175/2009JHM1066.1.

Santanello, J. A., C. D. Peters-Lidard, A. Kennedy, and S. V. Kumar (2013), Diagnosing the nature of land–atmosphere coupling: A case study of dry/wet extremes in the U.S. Southern Great Plains, *J. Hydrometeorol.*, *14*(1), 3–24, doi:10.1175/JHM-D-12-023.1.

Savijärvi, H. (1990), Fast radiation parameterization schemes for mesoscale and short-range forecast models, *J. Appl. Meteorol.*, *29*(6), 437–447, doi:10.1175/1520-0450(1990)029<0437:FRPSFM>2.0.CO;2.

Seneviratne, S. I., D. Lüthi, M. Litschi, and C. Schär (2006), Land-atmosphere coupling and climate change in Europe, *Nature*, *443*(7108), 205–9, doi:10.1038/nature05095.

Seneviratne, S. I., T. Corti, E. L. Davin, M. Hirschi, E. B. Jaeger, I. Lehner, B. Orlowsky, and A. J. Teuling (2010), Investigating soil moisture–climate interactions in a changing climate: A review, *Earth Sci. Rev.*, *99*(3–4), 125–161, doi:10.1016/j.earscirev.2010.02.004.

Siebesma, A. P., P. M. M. Soares, and J. Teixeira (2007), A combined eddy-diffusivity mass-flux approach for the convective boundary layer, *J. Atmos. Sci.*, *64*(4), 1230–1248, doi:10.1175/JAS3888.1.

Sippel, S., J. Zscheischler, M. D. Mahecha, R. Orth, M. Reichstein, M. Vogel, and S. I. Seneviratne (2016), Refining multi-model projections of temperature extremes by evaluation against land-atmosphere coupling diagnostics, *Earth Syst. Dynam. Discuss*, 1–24, doi:10.5194/esd-2016-48.

Smith, R. N. B. (1990), A scheme for predicting layer clouds and their water content in a general circulation model, *Q. J. R. Meteorol. Soc.*, *116*(492), 435–460, doi:10.1002/qj.49711649210.

Stocker, T. F., et al. (2013), Technical summary, in *Climate Change 2013: The Physical Science Basis. Working Group I Contribution to the Fifth Assessment Report of the Intergovernmental Panel on Climate Change*, edited by T. F. Stocker et al., Cambridge Univ. Press, Cambridge, U. K., and New York.

Stoy, P. C., et al. (2013), A data-driven analysis of energy balance closure across FLUXNET research sites: The role of landscape scale heterogeneity, *Agric. For. Meteorol.*, *171–172*, 137–152, doi:10.1016/j.agrformet.2012.11.004.

Taylor, C. M., R. A. M. de Jeu, F. Guichard, P. P. Harris, and W. A. Dorigo (2012), Afternoon rain more likely over drier soils, *Nature*, *489*(7416), 423–6, doi:10.1038/nature11377.

Tiedtke, M. (1989), A comprehensive mass flux scheme for cumulus parameterization in large-scale models, *Mon. Weather Rev.*, *117*(8), 1179–1800, doi:10.1175/1520-0493(1989)117<1779:ACMFSF>2.0.CO;2.

Tiedtke, M. (1993), Representation of clouds in large-scale models, *Mon. Weather Rev.*, *121*(11), 3040–3061.

Tompkins, A. M., K. Gierens, and G. Rädel (2007), Ice supersaturation in the ECMWF integrated forecast system, *Q. J. R. Meteorol. Soc.*, *133*(622), 53–63, doi:10.1002/qj.14.

Troen, I. B., and L. Mahrt (1986), A simple model of the atmospheric boundary layer: Sensitivity to surface evaporation, *Boundary Layer Meteorol.*, *37*(1–2), 129–148, doi:10.1007/BF00122760.

Van Den Hurk, B., and P. Viterbo (2000), Offline validation of the ERA40 surface scheme, *ECMWF Tech. Rep. no. 75*.

Van der Linden, P., and J. F. B. Mitchell (2009), ENSEMBLES: Climate change and its impacts: Summary of research and results from the ENSEMBLES project, *Met Off. Hadley Centre, FitzRoy Road, Exet. EX1 3PB, UK, 160*.

Vautard, R., et al. (2013), The simulation of European heat waves from an ensemble of regional climate models within the EURO-CORDEX project, *Clim. Dyn.*, *41*(9–10), 2555–2575, doi:10.1007/s00382-013-1714-z.

Wagner, W., W. Dorigo, R. de Jeu, D. Fernandez, J. Benveniste, E. Haas, and M. Ertl (2012), Fusion of active and passive microwave observations to create an Essential Climate Variable data record on soil moisture, *ISPRS Ann. Photogramm. Remote Sens. Spat. Inf. Sci.*, *I-7*, 315–321.

Wizemann, H., J. Ingwersen, K. Warrach-sagi, and V. Wulfmeyer (2015), Three year observations of water vapor and energy fluxes over agricultural crops in two regional climates of Southwest Germany, *Meteorol. Z.*, *24*(1), 39–59, doi:10.1127/metz/2014/0618.